

References

1. Lok AS, Liang RH, Chiu EK, Wong KL, Chan TK, Todd D. Reactivation of hepatitis B virus replication in patients receiving cytotoxic therapy. Report of a prospective study. *Gastroenterology*. 1991;100(1):182–8.
2. Hui CK, Cheung WW, Zhang HY, Au WY, Yueng YH, Leung AY, et al. Kinetics and risk of de novo hepatitis B infection in HBsAg-negative patients undergoing cytotoxic chemotherapy. *Gastroenterology*. 2006;131(1):59–68.
3. Yeo W, Chan TC, Leung NW, Lam WY, Mo FK, Chu MT, et al. Hepatitis B virus reactivation in lymphoma patients with prior resolved hepatitis B undergoing anticancer therapy with or without rituximab. *J Clin Oncol*. 2009;27(4):605–11 (Epub 2008/12/17).
4. Kusumoto S, Tanaka Y, Mizokami M, Ueda R. Reactivation of hepatitis B virus following systemic chemotherapy for malignant lymphoma. *Int J Hematol*. 2009;90(1):13–23 (Epub 2009/06/23).
5. Kusumoto S, Tanaka Y, Ueda R, Mizokami M. Reactivation of hepatitis B virus following rituximab-plus-steroid combination chemotherapy. *J Gastroenterol*. 2011;46(1):9–16 (Epub 2010/10/07).
6. Mitka M. FDA: increased HBV reactivation risk with ofatumumab or rituximab. *JAMA*. 2013;310(16):1664.
7. Ishida T, Utsunomiya A, Iida S, Inagaki H, Takatsuka Y, Kusumoto S, et al. Clinical significance of CCR4 expression in adult T-cell leukemia/lymphoma: its close association with skin involvement and unfavorable outcome. *Clin Cancer Res*. 2003;9(10 Pt 1):3625–34.
8. Ishii T, Ishida T, Utsunomiya A, Inagaki A, Yano H, Komatsu H, et al. Defucosylated humanized anti-CCR4 monoclonal antibody KW-0761 as a novel immunotherapeutic agent for adult T-cell leukemia/lymphoma. *Clin Cancer Res*. 2010;16(5):1520–31.
9. Yamamoto K, Utsunomiya A, Tobinai K, Tsukasaki K, Uike N, Uozumi K, et al. Phase I study of KW-0761, a defucosylated humanized anti-CCR4 antibody, in relapsed patients with adult T-cell leukemia–lymphoma and peripheral T-cell lymphoma. *J Clin Oncol*. 2010;28(9):1591–8.
10. Ishida T, Ueda R. Antibody therapy for Adult T-cell leukemia–lymphoma. *Int J Hematol*. 2011;94(5):443–52.
11. Ishida T, Joh T, Uike N, Yamamoto K, Utsunomiya A, Yoshida S, et al. Defucosylated anti-CCR4 monoclonal antibody (KW-0761) for relapsed adult T-cell leukemia–lymphoma: a multicenter phase II study. *J Clin Oncol*. 2012;30(8):837–42.
12. Motohashi K, Suzuki T, Kishimoto K, Numata A, Nakajima Y, Tachibana T, et al. Successful treatment of a patient with adult T cell leukemia/lymphoma using anti-CC chemokine receptor 4 monoclonal antibody mogamulizumab followed by allogeneic hematopoietic stem cell transplantation. *Int J Hematol*. 2013;98(2):258–60.
13. Nakano N, Kusumoto S, Tanaka Y, Ishida T, Takeuchi S, Takatsuka Y, et al. Reactivation of hepatitis B virus in a patient with adult T-cell leukemia–lymphoma receiving the anti-CC chemokine receptor 4 antibody mogamulizumab. *Hepatol Res*. 2014;44(3):354–7.
14. Shin IT, Tanaka Y, Tateno Y, Mizokami M. Development and public release of a comprehensive hepatitis virus database. *Hepatol Res*. 2008;38(3):234–43.
15. Hsu C, Tsou HH, Lin SJ, Wang MC, Yao M, Hwang WL, et al. Chemotherapy-induced hepatitis B reactivation in lymphoma patients with resolved HBV infection: a prospective study. *Hepatology*. 2014;59(6):2092–100.
16. Kusumoto S, Tanaka Y, Suzuki R, Watanabe T, Nakata M, Takasaki H, et al. Prospective nationwide observational study of hepatitis B virus (HBV) DNA monitoring and preemptive antiviral therapy for HBV reactivation in patients with B-cell non-Hodgkin lymphoma following rituximab containing chemotherapy: results of interim analysis. *Blood*. 2012; 120(21):abstract 2641.
17. Tsukasaki K, Utsunomiya A, Fukuda H, Shibata T, Fukushima T, Takatsuka Y, et al. VCAP-AMP-VECP compared with biweekly CHOP for adult T-cell leukemia–lymphoma: Japan Clinical Oncology Group Study JCOG9801. *J Clin Oncol*. 2007;25(34):5458–64.
18. Jo T, Ishida T, Takemoto S, Suzushima H, Uozumi K, Yamamoto K, et al. Randomized phase II study of mogamulizumab (KW-0761) plus VCAP-AMP-VECP (mLSG15) versus mLSG15 alone for newly diagnosed aggressive adult T-cell leukemia–lymphoma (ATL). *J Clin Oncol* 2013; 31: (suppl; abstr 8506).
19. Ishida T, Ueda R. Immunopathogenesis of lymphoma: focus on CCR4. *Cancer Sci*. 2011;102(1):44–50.
20. Oketani M, Ido A, Uto H, Tsubouchi H. Prevention of hepatitis B virus reactivation in patients receiving immunosuppressive therapy or chemotherapy. *Hepatol Res*. 2012;42(7):627–36 Epub 2012/06/13.
21. EASL clinical practice guidelines. Management of chronic hepatitis B virus infection. *J Hepatol*. 2012;57(1):167–85 Epub 2012/03/23.

CD30-positive primary bone marrow lymphoma mimicking Hodgkin lymphoma

Tomotaka Suzuki · Shigeru Kusumoto · Ayako Masaki · Takashi Ishida · Hiroshi Inagaki · Shinsuke Iida · Fumiko Mori

Received: 11 September 2014 / Revised: 18 November 2014 / Accepted: 19 November 2014 / Published online: 28 November 2014
© The Japanese Society of Hematology 2014

An 89-year-old Japanese man was admitted to this hospital for persistent fever for over 1 month and pancytopenia (a white blood cell count of 1700 / μ L with 46 % neutrophils, 33 % lymphocytes, 7 % atypical lymphocytes, and 14 % monocytes, a hemoglobin level of 8.4 g/dL, and a platelet count of 11.9×10^4 / μ L). A lymphoid neoplasm was suspected because of his markedly elevated soluble interleukin-2 receptor level of 16,709 U/mL, but computed tomography revealed no lymphadenopathy or hepatosplenomegaly. An 18 F-fluorodeoxyglucose positron emission tomography (FDG-PET) scan showed disseminated FDG uptake only in the bone marrow (Fig. 1).

Specimens of bone marrow aspiration and trephine biopsy showed hypercellular bone marrow and large binucleated or multinucleated cells resembling Reed-Sternberg (RS) cells, which were found sparsely in a background of small- to intermediate-sized lymphocytes and activated histiocytes (Fig. 2a). Bone marrow fibrosis was also seen. Immunostaining was carried out for various markers, including CD3, CD4, CD8, CD15 (Fig. 2b), CD20 (Fig. 2c), CD30 (Fig. 2d), CD45 (Fig. 2e), CD56, PAX5 (Fig. 2f), ALK, granzymeB, and BOB.1 (Fig. 2g), and

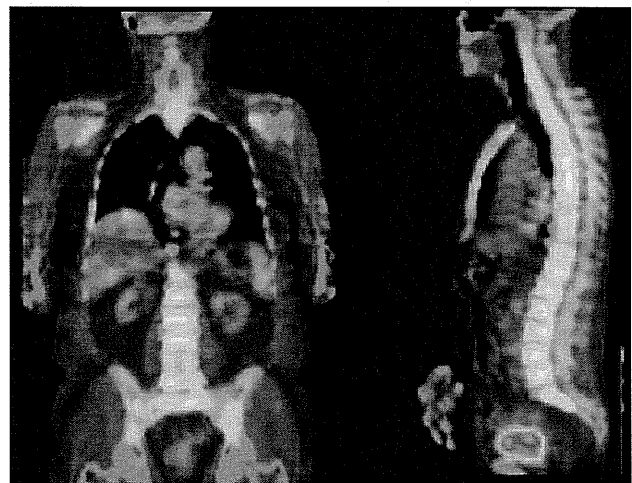


Fig. 1 This 18 F-fluorodeoxyglucose positron emission tomography scan shows disseminated FDG uptake in the bone marrow without evidence of the involvement of other organs. Focal weak FDG uptake in the liver and the spleen was considered to be within normal range

T. Suzuki (✉) · F. Mori
Department of Hematology, Toyokawa City Hospital, 23 Noji,
Yawata-cho, Toyokawa 442-8561, Japan
e-mail: let.me.be.92@gmail.com

S. Kusumoto · T. Ishida · S. Iida
Department of Hematology and Oncology, Nagoya City
University Graduate School of Medical Sciences, 1 Kawasumi,
Mizuho-chou, Mizuho-ku, Nagoya 467-8601, Japan

A. Masaki · H. Inagaki
Department of Pathology, Nagoya City University Graduate
School of Medical Sciences, 1 Kawasumi, Mizuho-chou,
Mizuho-ku, Nagoya 467-8601, Japan

nuclear staining for Epstein-Barr virus encoded RNA was performed by in situ hybridization (EBER-ISH). RS-like cells were positive for CD30, CD45, PAX5 and BOB.1. More specifically, a subset of the tumor cells was positive for BOB.1 but negative for the other antigens and EBER-ISH. The lymphocytes around the tumor cells were predominantly CD8-positive T-cells.

Southern blot analysis of the bone marrow did not reveal clonal rearrangements of the joining heavy chain immunoglobulin. On the other hand, polymerase chain reaction (PCR) of immunoglobulin heavy chain gene locus using D_H and J_H consensus primers demonstrated a monoclonal

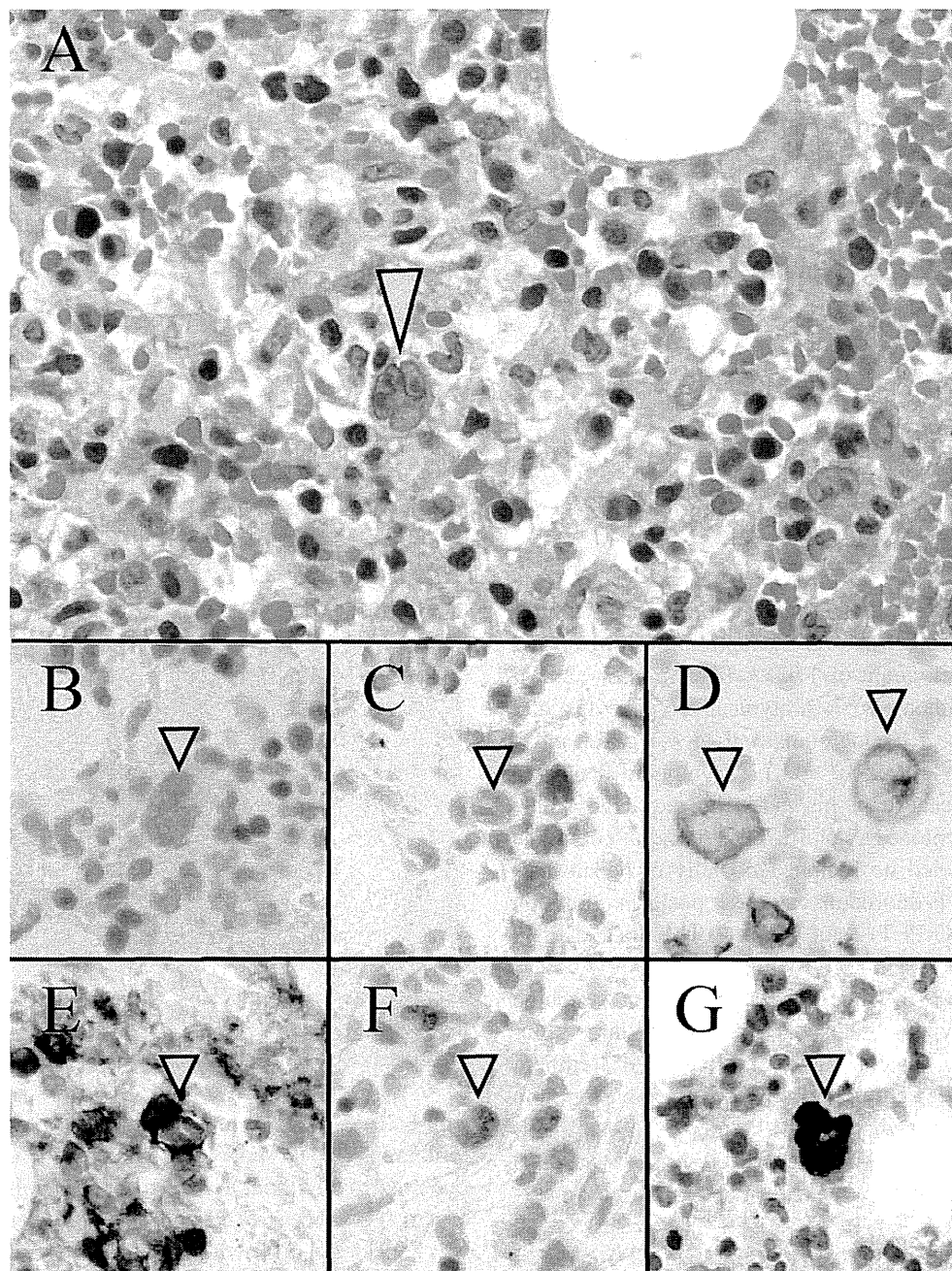


Fig. 2 Reed-Sternberg-like cells, indicated by *arrows*, are found sparsely in the bone marrow (**a** Hematoxylin and Eosin staining). These cells are negative for CD15 (**b**) and CD20 (**c**) but positive for

CD30 (**d**), CD45 (**e**) and PAX5 (**f**). Some neoplastic cells are positive for BOB.1 (**g**). (Original magnification of all panels, $\times 400$)

amplification product. Furthermore, cytogenetic study of the bone marrow showed an abnormal karyotype of 46,XY,del(3)(p?) in four of the 20 cells analyzed. Finally, the diagnosis of primary bone marrow large B cell lymphoma was established.

Descriptions of primary bone marrow lymphoma (PBML) in the literature have been limited, and its diagnostic criteria have not been established. Because our patient

did not show any evidence of organ involvement, other than bone marrow assessed by CT and PET scan, the diagnosis of PBML was thought to be reasonable.

In theory, RS-like cells should be interpreted carefully because they are not specific for Hodgkin lymphoma (HL) and have been found not only in cases of other malignancies, such as non-HL, carcinomas and sarcomas, but also in reactive processes. In the current case, HL was ruled

out because the RS-like cells were negative for CD15 and EBER-ISH but positive for CD45 and BOB.1.

A further question regarding the current case was the origin of the tumor cells and this was thought to be B lymphocytes, based on the positivity for PAX5 immunostaining, clonal

immunoglobulin heavy chain gene rearrangement detected by PCR analysis and negativity for NK/T-cell markers.

Conflict of interest The authors declare that they have no conflict of interest.

Immune-mediated antitumor effect by type 2 diabetes drug, metformin

Shingo Eikawa^{a,1}, Mikako Nishida^{a,1}, Shusaku Mizukami^a, Chihiro Yamazaki^a, Eiichi Nakayama^b, and Heiichiro Udono^{a,2}

^aDepartment of Immunology, Okayama University Graduate School of Medicine, Dentistry and Pharmaceutical Sciences, Okayama 700-8558, Japan; and ^bFaculty of Health and Welfare, Kawasaki University of Medical Welfare, Okayama 701-0193, Japan

Edited* by Douglas T. Fearon, University of Cambridge School of Clinical Medicine, Cambridge, United Kingdom, and approved December 29, 2014 (received for review September 12, 2014)

Metformin, a prescribed drug for type 2 diabetes, has been reported to have anti-cancer effects; however, the underlying mechanism is poorly understood. Here we show that this mechanism may be immune-mediated. Metformin enabled normal but not T-cell-deficient SCID mice to reject solid tumors. In addition, it increased the number of CD8⁺ tumor-infiltrating lymphocytes (TILs) and protected them from apoptosis and exhaustion characterized by decreased production of IL-2, TNF α , and IFN γ . CD8⁺ TILs capable of producing multiple cytokines were mainly PD-1⁻Tim-3⁺, an effector memory subset responsible for tumor rejection. Combined use of metformin and cancer vaccine improved CD8⁺ TIL multifunctionality. The adoptive transfer of antigen-specific CD8⁺ T cells treated with metformin concentrations as low as 10 μ M showed efficient migration into tumors while maintaining multifunctionality in a manner sensitive to the AMP-activated protein kinase (AMPK) inhibitor compound C. Therefore, a direct effect of metformin on CD8⁺ T cells is critical for protection against the inevitable functional exhaustion in the tumor microenvironment.

immune exhaustion | CD8T cells | antitumor immunity | tumor microenvironment | multifunctionality

In chronic infectious diseases and cancer, CD8⁺ T cells specific for viral and/or tumor antigens undergo repeated TCR stimulation because of persistent pathogens or cancer cells and gradually lose their ability to secrete IL-2, TNF α , and IFN γ , eventually undergoing apoptotic elimination in a process known as immune exhaustion (1). This worsening immune function is accompanied by phenotypic changes in CD8⁺ T cells, including the expression of exhaustion markers such as PD-1 and Tim-3 (2). Antitumor immunity is enhanced in mice deficient in PD-1 or its ligands PDL-1 and PDL-2 (2-4). Galectin 9, a Tim-3 ligand, is secreted by many tumor cells as well as by FoxP3-expressing regulatory T-cell (Treg) and inhibits Tim-3-expressing Th1 cells (5). An anti-Tim-3 antibody that blocks the galectin 9-Tim-3 pathway was found to accelerate antitumor immunity (6). Furthermore, the administration of blocking antibodies against both PD-1 and Tim-3 induced a more profound tumor rejection in comparison with that achieved with either antibody alone (7). The management of functional T-cell exhaustion within tumor tissues is currently an extensive focus in tumor immunotherapy (8, 9), together with efforts to neutralize immune-inhibitory Treg and myeloid-derived suppressor cell (MDSC).

Metformin (dimethylbiguanide) has been widely prescribed for type 2 diabetes. Its unique pharmacological features include its antihyperglycemic efficacy, which counters insulin resistance (10, 11). Early metformin use increases the survival of patients with obesity-involved type 2 diabetes and/or cardiovascular disease (12). In addition, recent reports have described the unexpected anticancer effects of metformin in patients with type 2 diabetes (13). Insulin-based diabetes treatment is associated with an increased cancer risk (14-17), whereas metformin use has been shown to decrease the frequency of specific cancers (18-21). Two independent metaanalyses of epidemiological studies concluded that compared with other treatments, metformin is

associated with a 30-40% reduction in the incidence of cancer among patients with type 2 diabetes, indicating the need to investigate the anticancer mechanisms of metformin and conduct long-term randomized controlled trials (RCTs) (22, 23).

In the HER-2/*neu* transgenic mouse breast cancer model, metformin treatment decreased the tumor burden and was associated with an increased life span (24). Combined use of metformin with chemotherapeutic agents such as cisplatin has also yielded clinical benefits (25, 26). Regarding the anticancer mechanism, metformin appears to preferentially kill cancer-initiating/stem cells from glioblastoma (27), breast (28) and ovarian cancers (29) via AMP-activated protein kinase (AMPK) activation.

In contrast to the inhibitory action of metformin on tumor cells, here we demonstrate the direct effects of metformin on CD8⁺ T cells, which eventually results in tumor growth inhibition. Metformin protects CD8⁺ tumor-infiltrating lymphocytes (TILs) from apoptosis, and the multifunctionality of exhausted PD-1⁻Tim-3⁺CD8⁺ TILs is restored via a shift from a central memory (TCM) to an effector memory T-cell (TEM) phenotype. This metformin-induced antitumor mechanism is therefore linked to marked changes in the characteristics of CD8⁺ TILs within the tumor microenvironment.

Results

Metformin-Induced Tumor Rejection Depends on CD8⁺T Cells. As metformin has been reported to decrease the rate of cancer incidence in type 2 diabetic patients, we at first examined whether

Significance

The multifunctional ability of CTLs is downregulated by interaction between immune-checkpoint molecules expressed on CTLs and their ligands expressed on cancer cells, referred to as immune exhaustion. The antibody-mediated, immune-checkpoint blockade turned out to a promising method for immunotherapy against advanced melanoma. Metformin, a drug prescribed for patients with type 2 diabetes, has been recognized to have anti-cancer effect. We found that CD8⁺ tumor infiltrating lymphocytes (TILs) is a target of metformin. CD8⁺ TILs inevitably undergo immune exhaustion, characterized by diminished production of multiple cytokines such as IL-2, TNF α , and IFN γ , followed by elimination with apoptosis. Metformin is able to counter the state. Along with conventional therapy, treatment of cancer patients with metformin may have a great advantage for cancer therapy.

Author contributions: H.U. designed research; S.E. and M.N. performed research; S.M., C.Y., E.N., and H.U. analyzed data; and H.U. wrote the paper.

The authors declare no conflict of interest.

*This Direct Submission article had a prearranged editor.

Freely available online through the PNAS open access option.

¹S.E. and M.N. contributed equally to this work.

²To whom correspondence should be addressed. Email: udono@cc.okayama-u.ac.jp.

This article contains supporting information online at www.pnas.org/lookup/suppl/doi:10.1073/pnas.1417636112/-DCSupplemental.

the drug could protect mice from methylchoranthrene-induced skin carcinogenesis. BALB/c mice were injected with 200 μg of methylchoranthrene on the right back and given 5 mg/mL metformin dissolved in the drinking water throughout the experiment. Significant inhibition of tumor development was observed in metformin-treated nondiabetic mice (Fig. S1A). We next attempted to determine whether metformin would be effective against an established solid tumor. Mice were intradermally injected with X-ray-induced RLmale1 leukemia cells and were provided oral metformin beginning on day 7. The tumors were gradually and completely rejected with no reappearance after metformin withdrawal. A rechallenge with more than twice the original number of the same tumor cells did not yield mass formation (Fig. 1A, *Left*), suggesting the generation of an immunologic memory response. Moreover, the antitumor effect was completely abrogated in SCID mice (Fig. 1A, *Right*), clearly demonstrating the necessity of T and/or B cells. Cytotoxic T lymphocytes (CTLs) specific for the tumor antigen peptide pRL1a (30) were generated in mice that rejected the tumor (Fig. S1B). Growth inhibition was observed with a metformin dose as low as 0.2 mg/mL (Fig. S1C). Of note, a previous report identified the achievement of plasma metformin concentrations of 0.45 and 1.7 $\mu\text{g}/\text{mL}$ using 1 and 5 mg/mL of metformin, respectively, in drinking water (31); these plasma concentrations are similar to those in patients with diabetes treated using metformin (0.5–2 $\mu\text{g}/\text{mL}$). Administration of metformin beginning on day 0, the time point of tumor inoculation, resulted in more effective rejection than on day 7. Beginning treatment on day 10 and 13 was also effective, although the effect was less than on day 0 (Fig. S1D). Finally, as expected, CD8⁺ but not CD4⁺ T cells were proven to be responsible for the antitumor effect, because their

depletion by mAb completely abrogated the response (Fig. 1B). Complete rejection by metformin was also observed with Renca (renal cell carcinoma), although partial but significant growth inhibition was observed with other tumors, 3LL (non small cell lung carcinoma), Colon 26 (intestinal carcinoma), and 4T1 (breast cancer) (Fig. S1 E–H).

Metformin Prevents Apoptosis of CD8⁺TILs, Irrespective of Expression of PD-1 and Tim-3. Injection of a vaccine consisting of antigen (Ag) and adjuvant primes and generates specific T-cell immunity, mainly in draining lymph nodes near the injection site. However, we did not inject tumor antigens with any kind of adjuvant in Fig. 1. Therefore, it is possible that a unique process occurs at the tumor site and leads to antitumor immunity. Based on this notion, we focused on TILs throughout the experiment to clarify the associated mechanism. We found that total numbers of TILs dramatically increased when metformin administration was started on day 7, and that both CD8⁺ and CD4⁺ T cells were involved in the increment (Fig. 1 C–E). In particular, the number of CD8⁺ TILs increased nearly fourfold. We considered the possibility that metformin may suppress expression of the immune exhaustion markers PD-1 and Tim-3 on CD8⁺ TILs, thus avoiding immune exhaustion. Therefore, we investigated the expression of these markers on CD8⁺ TILs derived from individual tumor-bearing mice (Fig. S1B). The number of PD-1⁺Tim-3⁺CD8⁺ TILs decreased from day 7–10, irrespective of metformin use (Fig. S2B). The PD-1⁺Tim-3⁺CD8⁺ TIL population increased progressively, whereas PD-1⁺Tim-3⁺CD8⁺ TILs remained stable. Metformin did not affect any subset populations (Fig. S2 B–E). However, we surprisingly found that a significant proportion of CD8⁺TILs underwent apoptosis, detected by

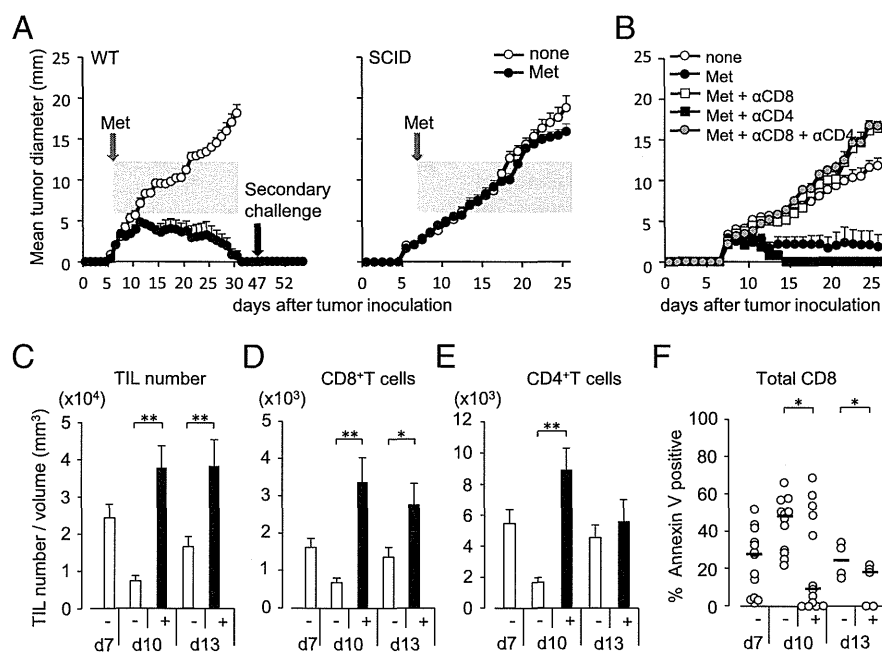


Fig. 1. Metformin suppressed tumor growth in vivo, depending on CD8⁺ T cells. (A) On day 0, BALB/c WT or SCID mice were intradermally inoculated with 2×10^5 RLmale1 cells on the right back. The mice received 5 mg/mL metformin (Met) or not (none) dissolved in the drinking water. The duration of Met administration is indicated by the shaded rectangle. The mean diameter of each tumor was measured every day and the data are plotted with SE. On day 45, Met-treated WT mice, all of which had rejected the tumor, were rechallenged with 5×10^5 RLmale1 cells. $n = 6$ in each group. The results are representative of two independent experiments. (B) Mice inoculated with RLmale1 were treated with metformin (Met) or not (none), starting on day 7 and i.v. injected with anti-CD8 mAb and/or anti-CD4 mAb on the same day. Average tumor diameters are plotted with SE. $n = 5$ in each group. (C–E) Mice inoculated with RLmale1 cells were treated with Met (+) or not (–) from day 7. On day 7, 10 and 13, the tumor mass was isolated and TILs were recovered. The numbers of TILs per tumor volume (mm^3) were calculated. The numbers of TIL (C), CD8⁺ (D), or CD4⁺ (E) per tumor volume are depicted. Also, the populations of CD8⁺TILs stained with Annexin V were plotted (F). All data were with SD ($n = 14$ on days 7 and 10, $n = 5$ on day 13). The horizontal bars indicate median values, and P values obtained by two-tailed Student's t test are shown as * $P < 0.05$, ** $P < 0.01$ $n = 5$ –14 in each group. Each symbol represents an individual mouse. The results depicted are a summary of three independent experiments.

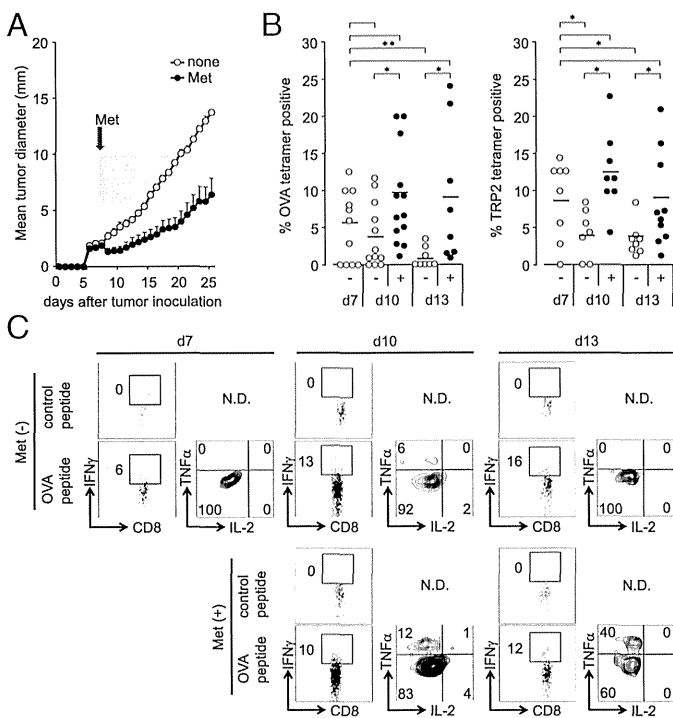


Fig. 2. Metformin improves the multifunctionality of antigen-specific CD8⁺ TILs in vivo. (A) Mice inoculated with 2×10^5 MO5 cells were treated with or without metformin from day 7, as indicated by the shadowed rectangle, and tumor growth was monitored. The results are representative of two independent experiments. $n = 5$ per group. (B) On days 7, 10, and 13, TILs were recovered from tumor masses and examined for K^b-OVA₂₅₇₋₂₆₄ and K^b-TRP2₁₈₀₋₁₈₈ tetramer binding ($n = 7-13$). (C) TILs recovered on days 7, 10, and 13 from five mice per group [with (+) or without (-) metformin] were pooled and stimulated with DC2.4 cells that had been prepulsed with OVA₂₅₇₋₂₆₅ peptide (10^{-6} M) for 8 h; TIL cytokine-producing ability was later examined.

Annexin V (Fig. 1F and Fig. S3A), and that metformin suppressed apoptosis induction in all subsets, including PD-1⁺Tim-3⁺CD8⁺TILs (Fig. S3B-E). Of note, the physiologically essential apoptotic process of CD4⁺CD8⁺ thymocytes, which depends on a mitochondrial pathway (32), was not down-regulated by metformin (Fig. S4), suggesting that an apoptotic mechanism unique to the tumor microenvironment is metformin-sensitive.

We next examined the metformin effects in another tumor system. MO5 is a subclone of B16 melanoma cells expressing ovalbumin (OVA) (33). Metformin administration induced significant antitumor activity (Fig. 2A). OVA- and TRP2-specific CD8⁺ TILs were identified by specific tetramers. Both TIL populations in untreated mice decreased gradually from day 7-13; in contrast, metformin administration maintained or increased these populations (Fig. 2B). CD8⁺ TILs again underwent apoptosis, which was suppressed by metformin administration (Fig. S5A and B). The Annexin V-positive populations among OVA tetramer-positive and -negative (includes TRP-2-positive population) CD8⁺ TILs were near 80% at day 10; however, metformin suppressed this rate to <20-40% (Fig. S5C and D). These results are consistent with those observed in the RLmale1 model. Next, to examine the functional state of antigen-specific TILs, magnet-purified CD8⁺ TILs isolated from tumor tissues were incubated with DC-like DC2.4 cells that had been pulsed with an epitope peptide (OVA₂₅₇₋₂₆₄); TILs were later examined for their cytokine production capacity. Only IFN γ -producing cells or very small populations producing both IFN γ and TNF α or IL-2 could be identified in untreated mice, whereas a marked increase in the population producing both IFN γ and TNF α was observed with metformin (Fig. 2C).

Influence of Metformin on the TCM/TEM Ratio of CD8⁺TILs. CD8⁺ TILs in the context of memory T cells are poorly understood. Elegant studies with an acute viral infection model have proposed classification of memory T cells into central memory (TCM; CD44⁺, CD62L^{high}) and effector memory (TEM; CD44⁺, CD62L^{low}) (34, 35). TCM were shown to mediate viral-specific recall responses. Based on this model, we investigated TCM and TEM CD8⁺ TILs. Without metformin, the staining of CD8⁺ TILs from an RLmale1 tumor using antibodies against CD62L and CD44 revealed that proportions of TCM and TEM were nearly equal on day 7 and 10 but shifted to TCM dominance on day 13. In contrast, metformin maintained TEM dominance from day 10 to day 13 (Fig. 3A). Further dissection of the TIL compartment based on CD62L and KLRG1 expression revealed that short-lived effector T cells (TE; CD62L^{low}KLRG1^{high}) were visible on day 7 but gradually decreased by day 13. In contrast, metformin yielded increases in both TEM and TE populations on day 13 (Fig. 3B), coinciding with tumor regression (Fig. 1A). In the MO5 model, metformin again caused TEM dominant over TCM (Fig. 3C and D). At this stage, we concluded that TEM and/or TE are more responsible than TCM for tumor rejection.

Metformin Induced Multifunctional CD8⁺ TEM Expressing the Exhaustion Marker Tim-3. We next investigated the capacity for triple cytokine (IL-2, TNF α , IFN γ) production or the multifunctionality of CD8⁺ TILs in the context of TCM/TEM classification. CD8⁺ TILs recovered from RLmale1 tumor masses were stimulated with PMA/ionomycin for 6 h in vitro and monitored for cytokine production. Without metformin, the cytokine-producing cells on day 10 were mainly identified as TCM (Fig. 4A). In contrast, with metformin, triple cytokine-producing cells appeared in correlation with the increased population of TEM (Fig. 4A). The populations with various cytokine producing patterns in the presence and absence of metformin are summarized in Fig. 4B. Metformin markedly changed the multifunctionality of CD8⁺ TILs. Taking these results together, we concluded that metformin-induced TEM capable of producing

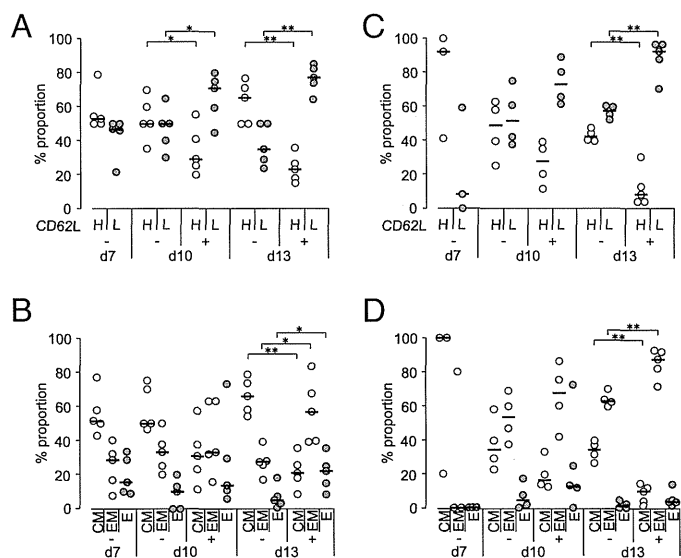


Fig. 3. Influence of metformin on the TCM/TEM ratio of CD8⁺ TILs. TILs were isolated on days 7, 10, and 13 from mice inoculated with RLmale1 (A and B, $n = 5$) or MO5 (C and D, $n = 3-5$) with (+) or without (-) metformin, and analyzed for CD8 and memory markers including CD44, CD62L, KLRG1. The proportion (%) of CD62L^{high} (H) and CD62L^{low} (L) among CD44⁺ cells in RLmale1 and MO5 models are shown in A and C, respectively. The proportion (%) of CD62L^{high}, KLRG1^{low} (central memory; CM) and CD62L^{low}, KLRG1^{low} (effector memory; EM) and CD62L^{low}, KLRG1^{high} (effector; E) in RLmale1 and MO5 are shown in B and D, respectively. * $P < 0.05$, ** $P < 0.01$.

multiple (triple and double) cytokines are most important for tumor rejection. We next classified CD8⁺ TILs on the basis of their expression of PD-1 and Tim-3, followed by intracellular cytokine staining. We found that CD8⁺ TILs with triple cytokine-producing abilities belonged exclusively to the PD-1⁻Tim-3⁺ subset, which was the supposedly exhausted population in the RLmale1 tumor model (Fig. S6). We further confirmed this notion using adoptive transfer experiments. MO5-inoculated mice were adoptively transferred with OT-I CD8⁺ T cells. The transferred T cells had been previously shown to undergo vigorous division and were thus cross-primed *in vivo* via the adjuvant-free administration of a fusion protein comprising OVA and *Mycobacterium* heat shock protein 70 (OVA-mHSP70) as a vaccine (36, 37). OVA-mHSP70 injection significantly enhanced the migration of the transferred CD45.1⁺OT-I CD8⁺ T cells into the tumor tissues; however, the cytokine-producing abilities of these cells were poor (Fig. 5A). In contrast, injection of the fusion protein together with oral metformin administration apparently improved the multifunctionality of the migrated T cells, which were classified as the Tim-3⁺ population (Fig. 5A).

Metformin-Treated Antigen-Specific Naive CD8 T Cells Migrate into Tumors and Exert Antitumor Immunity Following Adoptive Transfer.

It is unknown whether plasma metformin concentrations as low as 10 μ M (1.6 μ g/mL) would directly influence the fate of T cells. To address this important question, we incubated CD8⁺ T cells isolated from naive OT-I mice with 10 μ M metformin for 6 h in the presence or absence of different doses of the AMPK inhibitor compound C (38) as indicated (Fig. 5B). After extensive washing, the cells were transferred into MO5-bearing mice. Two days later, splenic T cells and TILs were recovered and investigated for the presence and multifunctionality of donor-derived CD8⁺ T cells. Metformin-treated CD8⁺ TILs comprised up to 9.9% of all CD8⁺ T cells and were identified as triple cytokine-producing cells (Fig. 5B). However, compound C treatment abrogated the migration, although donor CD8⁺ T cells were present in the spleens of all groups (Fig. 5B). Accordingly, tumor growth inhibition was apparent in the metformin-treated group, although this effect was blocked by compound C (Fig. 5C). The weak but significant metformin-mediated increase in the phosphorylation of AMPK and its downstream target acetyl-CoA carboxylase (ACC) and the abrogation of this effect by compound C were observed by Western blot analysis (Fig. 5D). The results led us to conclude that the direct action of metformin on CD8⁺ T cells, at least partly, reduced their exhaustion within the tumor microenvironment in a manner sensitive to the AMPK inhibitor compound C.

AMPK Phosphorylation, Enhanced Bat3 Expression, and Caspase-3 Inhibition Mediated by Metformin.

Finally, we examined the expression of CD8⁺ TIL molecules that may possibly be influenced by metformin administration. After CD8⁺ TIL purification on day 10, cell lysates were immediately prepared for candidate molecule detection via Western blot analysis and for caspase-3 activity measurement using a fluorescent substrate. The levels of phosphorylated AMPK α and β were increased; a twofold increase in Bat3 expression was also observed, whereas Bcl2 and Bax expression were unaltered (Fig. S7A). As expected, caspase-3 activity was prominent without metformin but was completely abrogated in CD8⁺ TILs from metformin-treated mice (Fig. S7B), which offers a plausible explanation for apoptosis inhibition. To further examine the apoptotic cell populations, we evaluated the expression of active caspase-3 in TCM, TEM, and TE. Without metformin, TCM, TEM, and TE all expressed active caspase-3 whereas with metformin, primarily TCM expressed this activated enzyme (Fig. S7C). These results may explain the dominance of TCM over TEM in the absence of metformin and the dominance of TEM and TE in the presence of metformin. pS6, a downstream target of mTOR, was positive in TCM, TEM, and TE without metformin but negative with metformin (Fig. S7D), indicating that metformin inhibits mTOR, possibly via AMPK activation.

Discussion

In this report, we showed that established solid tumors are regressed by oral administration of metformin, and that CD8⁺T cells mediate this effect. The number of FoxP3 expressing CD4⁺ regulatory T cells (Treg) has been implicated as a critical component in suppressing tumor immunity (39). However, their numbers were not decreased, rather, transiently increased by metformin administration in RLmale 1 tumor model (Fig. S8). Upon tumor rejection, the treated mice became resistant to rechallenge with the same tumor, providing proof of memory T-cell generation. Because no protective effect was observed in SCID mice, the direct killing of tumor cells by metformin is negligible. It was also confirmed by immunohistochemistry (IHC) of tumors. Tumors of mice treated with metformin showed decreased expression of Ki67 as a proliferation marker, accordingly, increased expression of active caspase 3 as an

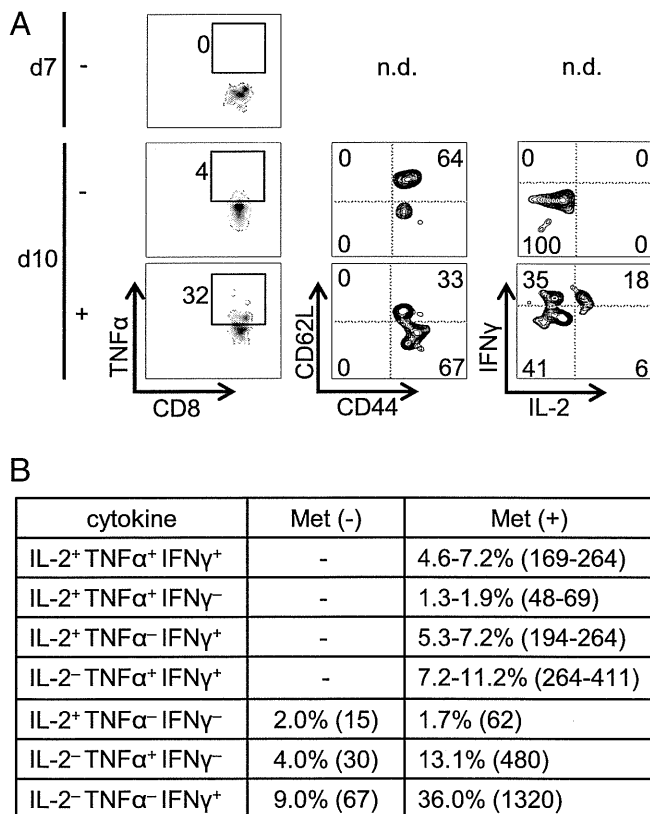


Fig. 4. Metformin-induced CD8⁺TILs with multifunctionality are TEM rather than TCM. (A) TILs were isolated on the indicated days from five mice per group inoculated with 2×10^5 RLmale1. Met treatment was started (+) or not (-) from day 7. TILs were then pooled on indicated days and stimulated with PMA/ionomycin for 6 h, stained for surface molecules including CD8, CD44, CD62L, followed by intracellular staining for IL-2, TNF α , and IFN γ . CD8⁺TILs producing TNF α were further analyzed for expression of CD62L and CD44 to identify TCM and TEM. Also, to investigate multifunctionality, cytokine-producing CD8⁺TILs were further examined for production of IFN γ and IL-2. (B) Summary of the populations of cytokine producing CD8⁺TILs on day 10 is shown. Gated populations for CD8⁺IFN γ ⁺, CD8⁺TNF α ⁺, or CD8⁺IL-2⁺ were further analyzed for their production of TNF α and IL-2, IFN γ and IL-2, or IFN γ and TNF α . The gating strategy gives rise to some ranges for % populations of double and triple cytokine producing TILs. The numbers within parenthesis indicate numbers of corresponding CD8⁺TILs per tumor volume (mm^3).

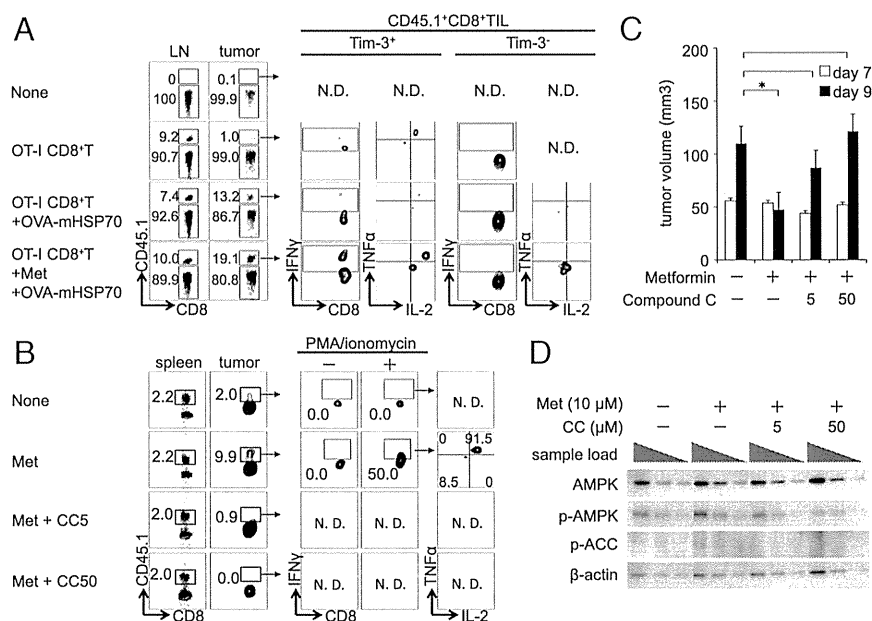


Fig. 5. Metformin use for combination with vaccine or cell therapy using CD8T cells. (A) Combined use of cancer vaccines and metformin improves CD8⁺ TIL multifunctionality. B6 mice (CD45.2) inoculated with 3×10^5 MO5 cells were adoptively transferred or not with 2×10^6 CD45.1/OT-I CD8⁺ T cells on day 7 ($n = 5$). Simultaneously, 10 μ g of the OVA-mHSP70 fusion protein were i.v. injected along with or without the oral administration of 5 mg/mL metformin as indicated. Three days later, the right inguinal lymph nodes (LNs) and tumor masses were removed, prepared as single-cell suspensions. The cells were stimulated with PMA/ionomycin, followed by labeling with antibodies and were subjected to flow cytometric analysis. (B) Metformin-treated antigen-specific naive CD8 T cells acquire multifunctionality within the tumor. B6 mice (CD45.2) inoculated with MO5 cells were adoptively transferred or not with 3×10^6 CD45.1/OT-I CD8 T cells on day 7 ($n = 5$). The cells to be transferred were isolated from CD45.1 OT-1 mice and precultured with 10 μ M metformin with or without compound C (5, 50 μ M) for 6 h before transfer. Two days later, the spleen and tumor tissues were removed and prepared as single-cell suspensions. The cells were then investigated for migration and multifunctionality. (C) The mean tumor diameters were measured on days 7 and 9 after MO5 inoculation and were plotted with SE. (D) The Western blot detection of AMPK, p-AMPK, and p-ACC in CD8⁺ T cells treated with metformin in vitro. Anti-actin was used as a loading control. OT-1 CD8 T cells treated in A were lysed, titrated 1-, 1/2-, and 1/4-fold, and subjected to the assay.

apoptosis marker; however, the effect was abrogated by CD8 T-cell depletion (Fig. S9). Our used model systems comprised highly immunogenic tumors, and it is unclear whether metformin would have the same effect on less immunogenic tumors. Demonstration of a similar effect in an autochthonous tumor model would be required in the future. Nonetheless, metformin countered apoptotic induction and reduced cytokine production in CD8⁺ TILs and thus blocked immune exhaustion within the tumor tissues we tested. The adoptive transfer experiment shown in Fig. 5 further demonstrated that the direct effect of metformin on CD8⁺ T cells, even at a physiologically relevant low concentration, markedly altered the cells' multifunctionality following migration into the tumor. Experiments with a genetic approach will be required to fully demonstrate whether this effect is mediated via AMPK activation in CD8⁺ T cells, because compound C is not highly specific for AMPK.

Dissection of TILs from the point of view of memory T cells in the context of multifunctionality provides mechanistic insight into metformin-induced antitumor immunity. Memory T cells have been classified as TCM, migrating between lymphoid organs, and TEM, circulating principally in the blood, spleen and peripheral tissues (34, 35, 40). In acute virus infection models, as the virus is cleared, the population of TCM progressively increase, whereas the total numbers of TEM rapidly decrease (41). The naturally occurring proportional shift from TEM to TCM, however, was not associated with metformin-induced rejection in the tumor models. For example, in the absence of metformin in the RLmale1 model, the TCM population gradually increased to exceed the TEM population by day 13 (Fig. 3A and B); however, this proportional shift to TCM was associated with progressive tumor growth rather than tumor regression. Metformin possibly affects the TCM/TEM ratio by regulating TEM apoptosis (Fig. S7C). The consequent

decreased TCM/TEM ratio was apparently associated with anti-tumor activity in both the RLmale1 and MO5 models.

Analysis of the cytokine-producing capacities of CD8⁺ TILs also revealed the importance of TEM over TCM. A significant proportion of the CD8⁺ TIL population was maintained by metformin and produced IL-2, TNF α , and IFN γ . These triple cytokine-producing CD8⁺ TILs were exclusively of the PD1⁻Tim3⁺ phenotype (Fig. S6), which is committed to a TEM rather than a TCM fate (Fig. 4). Moreover, although therapeutic vaccination with OVA-mHSP70 stimulated the migration of adoptively transferred OT-I CD8⁺ T cells into tumor tissues, these TILs lost multifunctionality (Fig. 5A). Possibly, the cells were exhausted from the tumor microenvironment. Coadministration of metformin, however, led to the activation of the migrated Tim3⁺ OT-I CD8⁺ T cells and the production of multiple cytokines (Fig. 5A). Therefore, combined use of metformin and cancer vaccines may improve the efficacy of the vaccine. These findings provide novel insights into anticancer immunity. It is possible that tumor persistence stimulates the development of CD8⁺ TILs into TCM cells, which will immediately become useless against tumor growth because of immune exhaustion, and that metformin counters this situation, leading to the conversion of TCM to activated-state TEM that are fully active against tumors, despite exhibiting the surface phenotype of an exhausted cell (e.g., Tim-3 expression).

A previous report found that metformin treatment following vaccination with attenuated *Listeria monocytogenes* expressing OVA (LmOVA) protected mice from challenge by tumor cells expressing OVA (42). This effect was caused by metformin-induced expansion of memory T cells after vaccination. As the tumor challenge occurred after metformin withdrawal, it is a matter of a prophylactic vaccination effect, which is different from the effects on immune exhaustion states in the tumor microenvironment.

mTOR inhibition is among the downstream consequences of AMPK signaling, which is activated by metformin. Therefore, rapamycin, an inhibitor of mTORC1, may share mechanistic effects with metformin. Rapamycin has been shown to promote the generation of memory T cells (42–44) particularly in viral infection models. A common feature in the results was the increased population of TCM over TEM consequent to rapamycin treatment (45). In our tumor models, however, metformin treatment preferentially increased the TEM population. It remains possible that additional pharmacological effects are involved in response to metformin versus rapamycin treatment. Further experiments will be required to elucidate cellular and molecular mechanism underlying metformin-induced reversion of exhausted CD8⁺TILs.

Materials and Methods

Mice. BALB/c and C57BL/6 (B6) mice were purchased from CLEA Japan and SLC. Breeding pairs of CB-17 SCID mice were provided by K. Kuribayashi, Mie University School of Medicine, Mie, Japan.

- Wherry EJ (2011) T cell exhaustion. *Nat Immunol* 12(6):492–499.
- Dong H, et al. (2002) Tumor-associated B7-H1 promotes T-cell apoptosis: A potential mechanism of immune evasion. *Nat Med* 8(8):793–800.
- Blank C, et al. (2004) PD-L1/B7H-1 inhibits the effector phase of tumor rejection by T cell receptor (TCR) transgenic CD8⁺ T cells. *Cancer Res* 64(3):1140–1145.
- Iwai Y, et al. (2002) Involvement of PD-L1 on tumor cells in the escape from host immune system and tumor immunotherapy by PD-L1 blockade. *Proc Natl Acad Sci USA* 99(19):12293–12297.
- Zhu C, et al. (2005) The Tim-3 ligand galectin-9 negatively regulates T helper type 1 immunity. *Nat Immunol* 6(12):1245–1252.
- Ngiow SF, et al. (2011) Anti-TIM3 antibody promotes T cell IFN- γ -mediated antitumor immunity and suppresses established tumors. *Cancer Res* 71(10):3540–3551.
- Sakuishi K, et al. (2010) Targeting Tim-3 and PD-1 pathways to reverse T cell exhaustion and restore anti-tumor immunity. *J Exp Med* 207(10):2187–2194.
- Sakuishi K, Jayaraman P, Behar SM, Anderson AC, Kuchroo VK (2011) Emerging Tim-3 functions in antimicrobial and tumor immunity. *Trends Immunol* 32(8):345–349.
- Pardoll DM (2012) The blockade of immune checkpoints in cancer immunotherapy. *Nat Rev Cancer* 12(4):252–264.
- Bailey CJ (1992) Biguanides and NIDDM. *Diabetes Care* 15(6):755–772.
- Bailey CJ, Turner RC (1996) Metformin. *N Engl J Med* 334(9):574–579.
- UK Prospective Diabetes Study (UKPDS) Group (1998) Effect of intensive blood-glucose control with metformin on complications in overweight patients with type 2 diabetes (UKPDS 34). *Lancet* 352(9131):854–865.
- McFarland MS, Cripps R (2010) Diabetes mellitus and increased risk of cancer: focus on metformin and the insulin analogs. *Pharmacotherapy* 30(11):1159–1178.
- Colhoun HM; SDRN Epidemiology Group (2009) Use of insulin glargine and cancer incidence in Scotland: a study from the Scottish Diabetes Research Network Epidemiology Group. *Diabetologia* 52(9):1755–1765.
- Currie CJ, Poole CD, Gale EA (2009) The influence of glucose-lowering therapies on cancer risk in type 2 diabetes. *Diabetologia* 52(9):1766–1777.
- Hemkens LG, et al. (2009) Risk of malignancies in patients with diabetes treated with human insulin or insulin analogues: A cohort study. *Diabetologia* 52(9):1732–1744.
- Jonasson JM, et al. (2009) Insulin glargine use and short-term incidence of malignancies—a population-based follow-up study in Sweden. *Diabetologia* 52(9):1745–1754.
- Bodmer M, Meier C, Krähenbühl S, Jick SS, Meier CR (2010) Long-term metformin use is associated with decreased risk of breast cancer. *Diabetes Care* 33(6):1304–1308.
- Evans JM, Donnelly LA, Emslie-Smith AM, Alessi DR, Morris AD (2005) Metformin and reduced risk of cancer in diabetic patients. *BMJ* 330(7503):1304–1305.
- Bowker SL, Majumdar SR, Veugelers P, Johnson JA (2006) Increased cancer-related mortality for patients with type 2 diabetes who use sulfonylureas or insulin. *Diabetes Care* 29(2):254–258.
- Libby G, et al. (2009) New users of metformin are at low risk of incident cancer: a cohort study among people with type 2 diabetes. *Diabetes Care* 32(9):1620–1625.
- Decensi A, et al. (2010) Metformin and cancer risk in diabetic patients: A systematic review and meta-analysis. *Cancer Prev Res (Phila)* 3(11):1451–1461.
- Noto H, Goto A, Tsujimoto T, Noda M (2012) Cancer risk in diabetic patients treated with metformin: a systematic review and meta-analysis. *PLoS ONE* 7(3):e33411.
- Anisimov VN, et al. (2005) Effect of metformin on life span and on the development of spontaneous mammary tumors in HER-2/neu transgenic mice. *Exp Gerontol* 40(8-9):685–693.

Tumor Cell Lines. BALB/c radiation leukemia RLmale1, B6 OVA-gene introduced B16 melanoma MO5, B6 nonsmall cell lung carcinoma 3LL, BALB/c intestinal carcinoma Colon 26, BALB/c renal cell carcinoma Renca, and BALB/c breast cancer cell 4T1 were used for the tumor assay. 3LL, Colon 26, Renca, and 4T1 were kindly provided by H. Yagita, Juntendo University School of Medicine, Tokyo, Japan.

Tumor Growth Assay. Mice were intradermally inoculated with 2×10^5 tumor cells (in 0.2 mL) on the right back with a 27-gauge needle. Before inoculation of tumor cells, the hair was cut with clippers. Mice were orally administered metformin hydrochloride (Wako) (5 mg/mL) or as indicated dissolved the drinking water. The diameter of the tumors was measured with Vernier calipers twice at right angles to calculate the mean diameter.

ACKNOWLEDGMENTS. We thank Ms. Yamashita for technical assistance and Dr. Toshifumi Matsuyama for critical reading of the manuscript and discussion about this work. This work was supported by grants from the Projects for Development of Innovative Research on Cancer Therapeutics by the Ministry of Education, Culture, Sports, Science, and Technology of Japan; Health and Labor Sciences Research Grants; Research on Applying Health Technology in Japan; The Naito Foundation; Takeda Science Foundation; and The Secom Science and Technology Foundation.

- Rocha GZ, et al. (2011) Metformin amplifies chemotherapy-induced AMPK activation and antitumoral growth. *Clin Cancer Res* 17(12):3993–4005.
- Hirsch HA, Iliopoulos D, Tschlis PN, Struhl K (2009) Metformin selectively targets cancer stem cells, and acts together with chemotherapy to block tumor growth and prolong remission. *Cancer Res* 69(19):7507–7511.
- Sato A, et al. (2012) Glioma-initiating cell elimination by metformin activation of FOXO3 via AMPK. *Stem Cells Transl Med* 1(11):811–824.
- Song CW, et al. (2012) Metformin kills and radiosensitizes cancer cells and preferentially kills cancer stem cells. *Sci Rep* 2:362.
- Shank JJ, et al. (2012) Metformin targets ovarian cancer stem cells in vitro and in vivo. *Gynecol Oncol* 127(2):390–397.
- Uenaka A, et al. (1994) Identification of a unique antigenic peptide pRL1 on BALB/c RL male 1 leukemia recognized by cytotoxic T lymphocytes and its relation to the Akt oncogene. *J Exp Med* 180(5):1599–1607.
- Memmott RM, et al. (2010) Metformin prevents tobacco carcinogen-induced lung tumorigenesis. *Cancer Prev Res (Phila)* 3(9):1066–1076.
- Hogquist KA, Baldwin TA, Jameson SC (2005) Central tolerance: Learning self-control in the thymus. *Nat Rev Immunol* 5(10):772–782.
- Ryu MS, et al. (2014) Accumulation of cytolytic CD8⁺ T cells in B16-melanoma and proliferation of mature T cells in TIS21-knockout mice after T cell receptor stimulation. *Exp Cell Res* 327(2):209–221.
- Sallusto F, Lenig D, Förster R, Lipp M, Lanzavecchia A (1999) Two subsets of memory T lymphocytes with distinct homing potentials and effector functions. *Nature* 401(6754):708–712.
- Masopust D, Vezyz V, Marzo AL, Lefrançois L (2001) Preferential localization of effector memory cells in nonlymphoid tissue. *Science* 291(5512):2413–2417.
- Suzue K, Zhou X, Eisen HN, Young RA (1997) Heat shock fusion proteins as vehicles for antigen delivery into the major histocompatibility complex class I presentation pathway. *Proc Natl Acad Sci USA* 94(24):13146–13151.
- Mizukami S, Kajiwara C, Tanaka M, Kaisho T, Udono H (2012) Differential MyD88/IRAK4 requirements for cross-priming and tumor rejection induced by heat shock protein 70-model antigen fusion protein. *Cancer Sci* 103(5):851–859.
- Zhou G, et al. (2001) Role of AMP-activated protein kinase in mechanism of metformin action. *J Clin Invest* 108(8):1167–1174.
- Onizuka S, et al. (1999) Tumor rejection by in vivo administration of anti-CD25 (interleukin-2 receptor α) monoclonal antibody. *Cancer Res* 59(13):3128–3133.
- Reinhardt RL, Khoruts A, Merica R, Zell T, Jenkins MK (2001) Visualizing the generation of memory CD4 T cells in the whole body. *Nature* 410(6824):101–105.
- Kedzierska K, Valkenburg SA, Doherty PC, Davenport MP, Venturi V (2012) Use it or lose it: establishment and persistence of T cell memory. *Front Immunol* 3:357.
- Pearce EL, et al. (2009) Enhancing CD8 T-cell memory by modulating fatty acid metabolism. *Nature* 460(7251):103–107.
- Araki K, et al. (2009) mTOR regulates memory CD8 T-cell differentiation. *Nature* 460(7251):108–112.
- Rao RR, Li Q, Odunsi K, Shrikant PA (2010) The mTOR kinase determines effector versus memory CD8⁺ T cell fate by regulating the expression of transcription factors T-bet and Eomesodermin. *Immunity* 32(1):67–78.
- Araki K, Youngblood B, Ahmed R (2010) The role of mTOR in memory CD8 T-cell differentiation. *Immunol Rev* 235(1):234–243.

Cytotoxic T Lymphocytes Block Tumor Growth Both by Lytic Activity and IFN γ -Dependent Cell-Cycle Arrest

Hirokazu Matsushita¹, Akihiro Hosoi^{1,2}, Satoshi Ueha³, Jun Abe³, Nao Fujieda^{1,2}, Michio Tomura⁴, Ryuji Maekawa², Kouji Matsushima³, Osamu Ohara⁵, and Kazuhiro Kakimi¹

Abstract

To understand global effector mechanisms of CTL therapy, we performed microarray gene expression analysis in a murine model using pmel-1 T-cell receptor (TCR) transgenic T cells as effectors and B16 melanoma cells as targets. In addition to upregulation of genes related to antigen presentation and the MHC class I pathway, and cytotoxic effector molecules, cell-cycle-promoting genes were downregulated in the tumor on days 3 and 5 after CTL transfer. To investigate the impact of CTL therapy on the cell cycle of tumor cells *in situ*, we generated B16 cells expressing a fluorescent ubiquitination-based cell-cycle indicator (B16-fucci) and performed CTL therapy in mice bearing B16-fucci tumors. Three days after CTL transfer, we observed diffuse infiltration of CTLs into the tumor with a large number of tumor cells arrested at the G₁ phase of the cell cycle, and the presence of

spotty apoptotic or necrotic areas. Thus, tumor growth suppression was largely dependent on G₁ cell-cycle arrest rather than killing by CTLs. Neutralizing antibody to IFN γ prevented both tumor growth inhibition and G₁ arrest. The mechanism of G₁ arrest involved the downregulation of S-phase kinase-associated protein 2 (Skp2) and the accumulation of its target cyclin-dependent kinase inhibitor p27 in the B16-fucci tumor cells. Because tumor-infiltrating CTLs are far fewer in number than the tumor cells, we propose that CTLs predominantly regulate tumor growth via IFN γ -mediated profound cytostatic effects rather than via cytotoxicity. This dominance of G₁ arrest over other mechanisms may be widespread but not universal because IFN γ sensitivity varied among tumors. *Cancer Immunol Res*; 3(1); 26–36. ©2014 AACR.

See related commentary by Riddell, p. 23

Introduction

Adoptive T-cell immunotherapy (ACT) using autologous tumor-infiltrating lymphocytes (TIL) can be highly effective for treating melanoma (1). The recent development of genetically engineered T cells stably expressing exogenous T-cell receptors (TCR) or chimeric antigen receptors (CAR) specific for tumor-associated antigens offers the possibility of testing the efficacy of ACT against a wide range of cancer types in addition to melanoma (2, 3). Many clinical trials have now been conducted using genetically engineered T cells specific for tumor antigens as well as TILs, and some objective responses have been achieved (4, 5). It is clear from mouse models that

adoptively transferred antigen-specific T cells are capable of eradicating established cancer (6–8), and the ability of CTLs to directly kill tumor and/or stromal cells is thought to be important for tumor elimination (9–11). Nonetheless, cytokines such as IFN γ and TNF α produced by T cells are also likely to contribute to the prevention of tumor growth by ACT via mechanisms other than cell lysis (12–14).

IFN γ is a critical cytokine for antitumor immunity under natural and therapeutic conditions (15, 16). It enhances tumor immunogenicity by upregulating components of the MHC antigen processing and presentation pathway. It also induces the expression of chemokines, including the angiostatic chemokines CXCL9 (MIG), CXCL10 (IP-10), and CXCL11 (I-TAC), that block neovascularization in the tumor and recruit effector immune cells (17–19). Furthermore, IFN γ has been reported to exert antiproliferative effects on the developing tumor (20, 21), and it triggers apoptosis of tumor cells by inducing proapoptotic molecules (22, 23).

To understand the global antitumor effect mediated by ACT, we used the B16 melanoma pmel-1 TCR-transgenic T-cell model to perform a gene expression analysis of ACT-treated tumors. On the basis of these results, we focused on genes controlling the cell cycle and arresting growth of B16 tumor cells in this model. We examined the effects on tumor cells of the IFN γ produced by the CTLs *in situ* using cell-cycle status indicators and investigated the mechanism of cell-cycle arrest. Furthermore, we demonstrate the importance of cell-cycle arrest induced by CTL-derived IFN γ in the regulation of tumor growth.

¹Department of Immunotherapeutics, The University of Tokyo Hospital, Tokyo, Japan. ²Medinet Co Ltd., Yokohama, Japan. ³Department of Molecular Preventive Medicine, Graduate School of Medicine, The University of Tokyo, Tokyo, Japan. ⁴Center for Innovation in Immunoregulative Technology and Therapeutics, Kyoto University Graduate School of Medicine, Kyoto, Japan. ⁵Department of Human Genome Research, Kazusa DNA Research Institute, Chiba, Japan.

Note: Supplementary data for this article are available at Cancer Immunology Research Online (<http://cancerimmunolres.aacrjournals.org/>).

Corresponding Author: Kazuhiro Kakimi, Department of Immunotherapeutics, The University of Tokyo Hospital, 7-3-1 Hongo, Bunkyo-Ku, Tokyo 113-8655, Japan. Phone: 81-3-5805-3161; Fax: 81-3-5805-3164; E-mail: kakimi@m.u-tokyo.ac.jp

doi: 10.1158/2326-6066.CIR-14-0098

©2014 American Association for Cancer Research.

Materials and Methods

Mice, tumor cells, and peptides

Six-week-old male C57BL/6 mice were purchased from Japan SLC. Mice transgenic for the pmel-1-TCR, which recognizes the H-2D^b-restricted epitope EGSRNQDWL from gp100 (gp100₂₅₋₃₃), were obtained from The Jackson Laboratory. All mice were housed in a pathogen-free environment, and all animal procedures were conducted in accordance with institutional guidelines. All animal experiments were approved by the University of Tokyo Ethics Committee for Animal Experiments (10-P-127). The H-2D^b-restricted peptide human gp100 (hgp100₂₅₋₃₃, KVPRNQDWL) was purchased from GenScript Japan at a purity of >90%, with free amino and carboxyl terminals. B16F10, FBL3, and 3LL cell lines were maintained in culture medium consisting of DMEM with 10% FCS, 100 U/mL penicillin, and 100 μ g/mL streptomycin. EL4, P815, and CT26 were cultured in RPMI-1640 medium supplemented with 10% FCS, 100 U/mL penicillin, and 100 μ g/mL streptomycin. All cell lines were tested for Mycoplasma by the MycoAlert Mycoplasma Detection kit (Lonza). Cellular morphology and growth curve *in vitro* were checked in all cell lines. B16F10 and B16-fucci cells were authenticated by transplantation for assessing growth ability *in vivo*.

Dendritic cell preparation and CTL stimulation

Dendritic cells (DC) were obtained by 8-day culture of C57BL/6-derived bone marrow cells with granulocyte-macrophage colony-stimulating factor (GM-CSF), as described previously (24). Briefly, bone marrow cells obtained from tibias and femurs of C57BL/6 mice were cultured in RPMI-1640 medium supplemented with 10% FCS, 10 mmol/L HEPES, 5 \times 10⁻⁵ mol/L 2-mercaptoethanol, 1 \times 10⁻³ mol/L sodium pyruvate, 1% nonessential amino acids, 100 U/mL penicillin, 100 μ g/mL streptomycin, and 20 ng/mL GM-CSF (PeproTech) for 8 days. On days 3 and 6, half of the medium was replaced with fresh medium containing GM-CSF. DCs were further incubated with 1 μ g/mL lipopolysaccharide for 16 hours and then pulsed with 1 μ g/mL hgp100 peptide for 3 hours to obtain mature DCs. To prepare CTLs, 1 \times 10⁷ spleen cells from pmel-1 TCR-transgenic mice were cocultured with 2 \times 10⁵ DCs in a medium containing 50 U/mL IL2 (Chiron Corporation). After 3 days of *in vitro* stimulation, approximately 90% of the harvested cells were CD3⁺CD8⁺ CTLs.

ACT and anti-IFN γ mAb treatment

C57BL/6 mice were inoculated subcutaneously with 1 \times 10⁶ B16 tumor cells followed by adoptive CTL transfer (1 \times 10⁷ or 4 \times 10⁷) 9 days later. Tumor growth was monitored every 2 to 3 days with calipers in an anonymous fashion. On the day of, and 2 days after, CTL transfer, mice received intraperitoneal injections of 500 μ g anti-IFN γ mAb (clone XMG1.2; BioXCell) or rat IgG₁ isotype control (BioXCell). Tumor volume was calculated as described previously (24).

Cell preparation and flow cytometry

Tumors were harvested from mice at scheduled time points, cut into pieces, and resuspended in Hank's Balanced Salt Solution (HBSS) supplemented with 0.1% collagenase D (Roche Diagnostics) and DNase I (Roche Diagnostics) for 60 minutes at 37°C. The entire mass of the material was pressed through a 70- μ m cell strainer (BD Falcon; BD Biosciences) using a plunger to obtain single-cell

suspensions of tumor-infiltrating cells. For flow cytometry, the cells were first stained with the Fixable Viability Dye eFluor450 (eBioscience) to label dead cells, and pretreated with Fc Block (anti-CD16/32 clone 2.4G2; BD Pharmingen). The cells were then stained with antibodies and analyzed on a Gallios flow cytometer (Beckman Coulter). The following mAbs were obtained from BioLegend: PerCP/Cy5.5-conjugated anti-CD45, Alexa Fluor647-conjugated anti-CD90.1, and APC-Cy7-conjugated anti-CD8. Data were analyzed with the Kaluza software (Beckman Coulter).

Comprehensive gene expression analysis

Gene expression profiling data of B16 tumor tissues on different days were obtained by Agilent whole-mouse genome microarray. Total RNA was extracted with TRizol (Invitrogen) from B16 tumor tissues and fluorescently labeled using a One-Color Agilent Quick Amp Labeling Kit. The microarray slides were hybridized, washed, and read on an Agilent Microarray scanner following the manufacturer's instructions, and raw fluorescence signal intensities were generated by Agilent Feature Extraction Software v9.5. The signals were normalized to align at 75th percentile, and then turned into log₂ ratio against day 1 in untreated and CTL-treated groups. We began with 45,018 probes, and removed probes if their glsWellAboveBG flag values were 0 at all samples, and then filtered out log₂ ratio values that were unvarying (between -1 and 1) at all time points. We obtained 10,855 probes and ran hierarchical clustering (standard correlation, UPGMA) on them. All data were analyzed with the Subio Platform and Basic Plug-in v1.16 (Subio Inc.). The microarray data are available from the Gene Expression Omnibus (GEO) database (series accession number GSE57304; sample accession numbers GSM1379331–GSM1379344).

For quantitative gene panel-based PCR, Cell Cycle RT² Profiler PCR arrays (SABioscience; http://www.sabiosciences.com/rt_pcr_product/HTML/PAMM-020Z.html) were used to simultaneously examine the mRNA levels of 84 genes in 96-well PCR array plates. Total RNA was prepared using TRizol according to the manufacturer's instructions (Invitrogen), and reverse-transcribed using RT2 First Strand kits (SABioscience). Real-time PCR was performed as instructed by the supplier on an ABI PRISM 7900HT Sequence Detection System (Life Technologies). Data were analyzed by a $\Delta\Delta$ cycle threshold method to determine the fold changes of the mRNA levels (<http://www.SABiosciences.com/pcrarraydataanalysis.php>).

Expression vectors

CSII-EF-MCS/mAG-hGeminin and CSII-EF-MCS/mKO-cdt1 vectors were kindly provided by Dr. Atsushi Miyawaki (RIKEN, Wako, Japan; ref. 25). cDNA encoding mouse *IFNGR1* lacking the intracellular component of the receptor (26) was generated by PCR using the primer pair 5'-ATCTCACTCGAGATGGGCCCG-CAGGCGGCAGCT-3' and 5'-ATCTCAGAATTCATTCTTCTTAG-TATACCAATA-3' and subcloned into the *Xho*-1 and *Eco*-RI sites of the RV-GFP vector (designated RV-IFNGR1 Δ IC; ref. 27).

Production of B16-fucci and B16-fucci Δ IC tumor cells

mAG-hGeminin and mKO-cdt1 were expressed in B16 tumor cells using lentiviral vectors (designated B16-fucci). IFNGR1 lacking the sequence encoding the intracellular component of the receptor was expressed in B16-fucci tumor cells in the same way (designated B16-fucci Δ IC).

Matsushita et al.

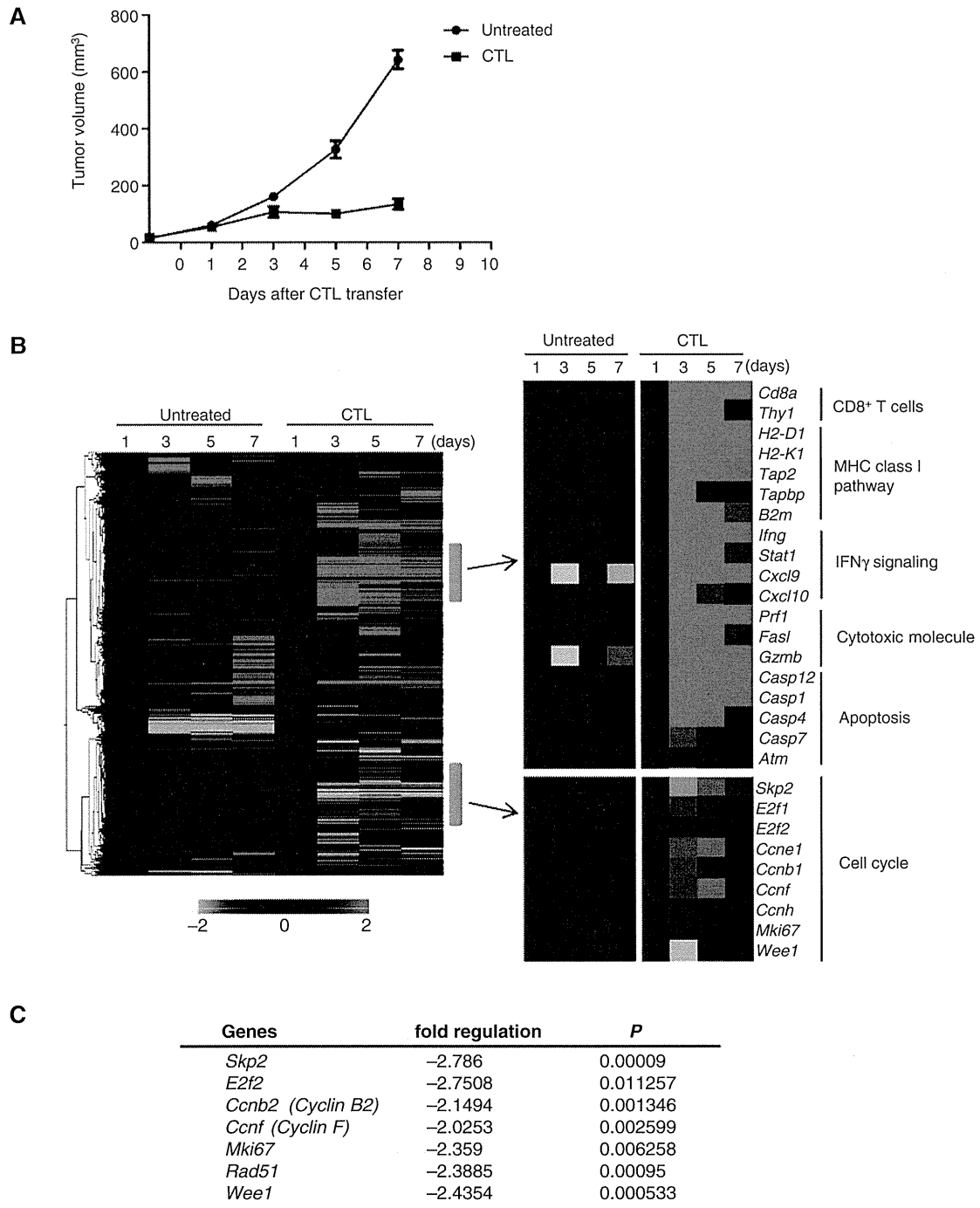


Figure 1. Gene expression analysis of the tumor in ACT. A, C57BL/6 mice were injected with 1×10^6 B16 tumor cells, and 9 days later (designated as day 0), tumor-bearing mice received 1×10^7 *in vitro* activated B16-specific (gp100-specific) CD90.1⁺ CTLs (designated ACT mice). Tumor volumes were measured on days 1, 3, 5, and 7 after CTL transfer ($n = 5$). B, tumor tissues from untreated or ACT mice were harvested on days 1, 3, 5, and 7. Total RNA extracted from 3 to 4 tumor tissues in each group was pooled and used for gene expression analysis. Heatmaps of hierarchical clustering analysis based on fold changes of gene expression on days 3, 5, and 7 relative to day 1 are shown (left). Some groups of genes that were upregulated (top) or downregulated (bottom) after CTL transfer were extracted (right). C, cell-cycle PCR array performed using tumor tissues from untreated or ACT mice ($n = 4$) on day 3. Seven cell-cycle genes that were significantly downregulated in the tumors from ACT mice are shown. The fold regulation is the negative inverse of the fold change.

Quantitative RT-PCR

Total RNA was extracted using TRizol and converted into cDNA using the SuperScript III First-Strand Synthesis System according to the manufacturer's instructions (Invitrogen). Quantitative RT-PCR (qRT-PCR) reactions were carried out using EXPRESS SYBR GreenER qPCR SuperMix Universal (Invitrogen). Primer sequences are listed in Supplementary Table S1. PCR reactions were run in a Thermal Cycler Dice Real-Time System TP800 (TaKaRa) using the following program: one cycle of 95°C for 2 minutes, 40 cycles at 95°C for 15 seconds, and 60°C for 30 seconds. Results are expressed as ratios. The quantity of target mRNA was normalized to the level of GAPDH in each sample. PCR was performed in duplicate for each experiment, and PCR products were monitored by electrophoresis in 1.8% agarose gels and visualized with ethidium bromide.

Histologic analysis

Cryosections were fixed in 4% paraformaldehyde (PFA) at 4°C overnight and then transferred into 30% sucrose/PBS. After incubation for more than 24 hours, they were embedded in an optimal cutting temperature (OCT) compound (Sakura Finetek Japan) in liquid nitrogen. Sections measuring 8–10 μ m were incubated with primary antibodies, followed by secondary antibodies and streptavidin. Polyclonal anti-Azami-Green antibody (PM011) was purchased from MBL. Polyclonal anti-single-stranded DNA was purchased from IBL-America. APC-conjugated anti-CD90.1 antibody was purchased from BD Biosciences. Alexa 647-conjugated polyclonal secondary antibodies and streptavidin were from Life Technologies. Anti-APC-biotin was from BioLegend. The samples were analyzed using a BZ-9000 fluorescence microscope with BZ-II image processing software (Keyence). The number of cells in the necrotic/apoptotic area was estimated by calculating the surface area of the region using BZ-H1M software (Keyence).

Cytology

Cultured B16-fucci tumor cells treated with IFN γ were examined using bright-field or fluorescence microscopy (Olympus IX71; Olympus; magnification, \times 200).

Senescence-associated β -galactosidase activity assay

Senescence-associated β -galactosidase (SA- β -gal) activity in cancer cells was assessed using the Senescence Detection Kit (BioVision). SA- β -gal-positive cells were identified using bright-field microscopy (Olympus IX71; Olympus; magnification, \times 400).

Protein extraction and Western blotting

B16-fucci tumors were harvested from untreated or ACT mice receiving either rat IgG (control for treatment) or anti-IFN γ mAb on day 3 after CTL transfer. Protein extracts were prepared from each tissue using RIPA buffer (Thermo Scientific) with the protease inhibitor cocktail Complete Mini (Roche). Protein extracts (50 μ g) were used for immunoblotting. Protein extracts (30–50 μ g) from B16-fucci, B16-fucci Δ IC cells, FBL3-, or EL4-treated with IFN γ (10 U/mL) for the indicated time were used for immunoblotting. The following antibodies, all from Santa Cruz Biotechnology, were used: rabbit anti-pSTAT1 (sc-7988-R), rabbit anti-Skp2 (sc-7164), mouse anti-ATM (sc-23921), rabbit anti-p53ser15 (sc-101762), and rabbit anti-p21 (sc-397). Mouse anti-

p27 (kip1) antibody was purchased from BD Biosciences. All antibodies were used at a final concentration of 0.2 to 1.0 μ g/mL. After incubation with anti-rabbit IgG or anti-mouse IgG antibodies conjugated with horseradish peroxidase, proteins were visualized using the ECL Plus Western Blotting Detection System (GE Healthcare Life Sciences).

Statistical analysis

Comparison of results was performed by an unpaired, two-tailed Student *t* test with GraphPad Prism 5 (GraphPad Software, Inc.).

Results

Gene expression analysis in CTL transfer therapy

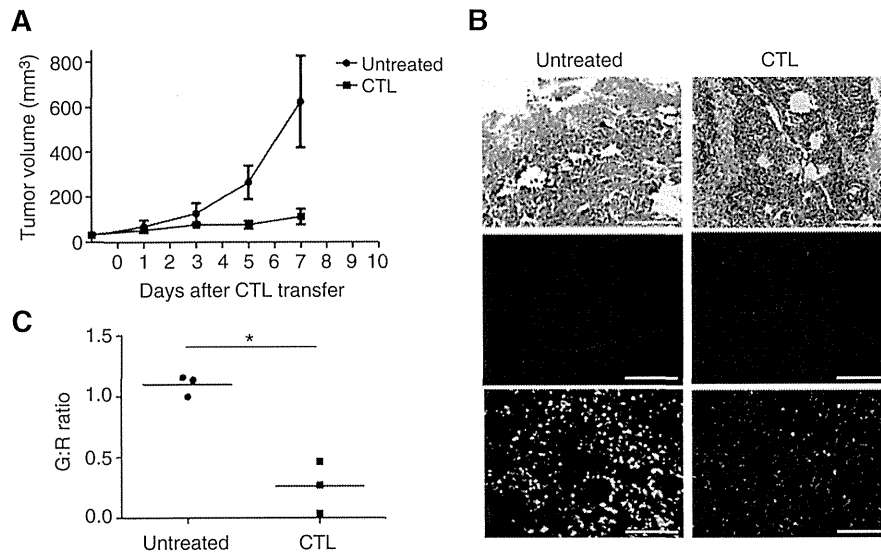
To understand the effector mechanism whereby ACT inhibits tumor growth, we assessed tumor-cell gene expression in a B16 melanoma model of pmel-1 TCR-transgenic CTL transfer. Tumors grew progressively in untreated B16-bearing mice, which was prevented between days 3 and 7 after the animals had received 10 million CTLs (Fig. 1A and Supplementary Fig. S1A). Tumor tissues were harvested from untreated mice and ACT mice on days 1, 3, 5, and 7 after CTL transfer, and gene expression was analyzed. Upregulation of genes related to CD8⁺ T cells, the MHC class I pathway, IFN γ signaling, cytotoxic effector molecules, and others was observed in tumors from treated but not untreated mice (Fig. 1B). These data are consistent with our previous findings (24, 28) that adoptively transferred CTLs infiltrated into the tumor and that mRNA encoding IFN γ , *Perforin*, *Granzyme B*, and *FasL* was expressed on days 3 to 7, with kinetics reflecting the infiltration of the CTLs (Supplementary Fig. S1B and S1C).

Interestingly, some genes positively regulating the cell cycle, such as *Skp2*, *E2f2*, *Ccnf*, *Mki67*, and *Wee1*, were downregulated in tumors from ACT mice on days 3 and 5 (Fig. 1B). This was not the case in the untreated controls. We confirmed these data by a cell-cycle PCR array (Fig. 1C). Thus, gene expression analysis revealed profiles related to cell-cycle regulation, as well as cytotoxicity, in tumors from mice with ACT treatment.

CTL therapy induces G₁ cell-cycle arrest

Using the fucci (fluorescent ubiquitination-based cell-cycle indicator) system (25), we investigated the impact of ACT on the cell cycle of B16 tumor cells. To this end, we generated B16 tumor cells expressing fucci (designated B16-fucci), which emit red fluorescence in the G₁-phase, but otherwise fluoresce green. We then treated B16-fucci tumor-bearing mice with ACT. Tumor growth was not affected by the transduction of fucci into B16 tumor cells, but ACT inhibited their growth (Fig. 2A). On day 3 after CTL transfer, tumors were harvested from untreated or ACT mice for histologic analysis. As shown in Fig. 2B, CTLs had infiltrated into the tumors and were visible as blue spots. Whereas green cells were dominant in the growing tumor cells, the majority of tumor cells from ACT mice were red, suggesting that CTL therapy induced tumor cell-cycle arrest in the G₁-phase. Expressing the cell-cycle state as a green:red (G:R) ratio (Fig. 2C) showed that this was lower in the ACT mice (0.26 ± 0.12 ; $n = 3$) than in the untreated control mice on day 3 (1.1 ± 0.05 ; $n = 3$; $P = 0.0032$). This difference remained up to day 5 after CTL transfer, but on day 7, the G:R ratio increased again, together with the disappearance of CTLs, and green cells became dominant once more after day 10 (Supplementary Fig. S1B).

Matsushita et al.

**Figure 2.**

CTL transfer therapy induced G_1 cell-cycle arrest of the tumor. A, C57BL/6 mice were injected with 1×10^6 B16-fucci tumor cells, and 9 days later, tumor-bearing mice ($n = 5$) were treated as described in Fig. 1. B, representative hematoxylin and eosin (top) and fluorescence microscopy images (middle and bottom) of cryosections of B16-fucci on day 3 ($n = 3$ per group). Alexa Fluor647-labeled anti-mouse CD90.1 antibody was used to detect infiltrating CD90.1⁺ T cells (blue cells; middle). Scale bars, 200 μm . C, analysis of cell-cycle stage was performed by calculating the G:R ratio in fluorescence images ($n = 3$ per group). Samples were compared using an unpaired, two-tailed Student t test (*, $P < 0.01$).

IFN γ is critical for tumor growth inhibition and cell-cycle arrest

IFN γ is important for antitumor immunity. We have shown that it is critical for tumor growth inhibition in this model using IFN γ neutralizing antibody (anti-IFN γ mAb; ref. 28). Because IFN γ is involved in MHC class I upregulation, antigen processing, and trafficking of T cells into the tumor site by promoting chemokine production, the number of T cells infiltrating into the tumor was decreased by neutralizing IFN γ (data not shown). It was necessary to inject 4-fold more T cells to achieve the same level of CTL infiltration in anti-IFN γ Ab-treated animals (Fig. 3B). Nevertheless, anti-IFN γ treatment still prevented tumor growth blockade, despite the presence of equivalent levels of CTL in the tumor (Fig. 3A). Strikingly, this was the case even though the expression of mRNA encoding the effector molecules *IFN γ* , *Perforin*, *Granzyme B*, and *FasL* in ACT mice treated with anti-IFN γ mAb was the same or even higher than that in control ACT mice treated with rat IgG (Fig. 3C and D). A major difference in the anti-IFN γ mAb-treated mice was that the expression of mRNA encoding *STAT1* and IFN γ -inducible genes such as *MIG*, *IP10*, or *I-TAC* was suppressed. This suggests that IFN γ signaling was blocked by the treatment with anti-IFN γ mAb.

As shown in Fig. 4A, all tumor cells fluoresced either green or red. In growing tumors, the majority of B16 tumor cells were in the S–G₂–M phase (Fig. 4A, left). After CTL transfer, most of the tumor cells became red (Fig. 4A, middle), but in the anti-IFN γ mAb-treated ACT mice, the tumor cells remained green (Fig. 4A, right). Diffused infiltration of CTLs into the tumor accompanied by massively infiltrated mononuclear cells and destruction of tumor cells, corresponding to spotty necrotic/apoptotic areas, was seen in ACT mice whether or not they received anti-IFN γ mAb treatment. Furthermore, apoptotic cells positive for single-stranded DNA (ssDNA), detected as white spots, were rare, but were present equally in ACT mice with or without anti-IFN γ mAb treatment (Fig. 4B and C). This, therefore, suggests that the transferred CTLs actually mediated relatively little tumor cell killing, which was unaffected by anti-IFN γ mAb administration.

The numbers of CTLs, tumor cells in necrotic/apoptotic areas, and tumor cells in the G₁ or S–G₂–M phase were compared

systematically in these mice. More green than red cells were observed in untreated tumors (Fig. 4D). In CTL-treated tumors, as described above, the G:R ratio was inverted, but the ratio was restored by the abrogation of IFN γ signaling. The surface area of the part of the tumor with necrotic/apoptotic cells was similar in the two CTL-treated groups (with or without anti-IFN γ mAb treatment), and the estimated number of dead cells was always smaller than that of the live cells (whether green or red; Fig. 4E). These results indicate that G₁ cell-cycle arrest, and not cytolytic killing, was primarily responsible for the CTL-induced suppression of tumor growth.

IFN γ directly suppress B16-fucci tumor cell growth through cell-cycle arrest

We constructed B16-fucci tumor cells expressing an IFN γ receptor lacking the intracellular component (B16-fucci Δ IC). ACT did not suppress the growth of these cells even when 4-fold more CTLs (4×10^7) were transferred (Supplementary Fig. S2A). Although a similar number of CTLs infiltrated into B16-fucci Δ IC tumor sites, as in mice with B16-fucci tumors receiving 4-fold less CTLs, no IFN γ production was observed (Supplementary Fig. S2B and S2C), and therefore the effect of IFN γ could not be evaluated in this system. This might be due to limited recognition of B16-fucci Δ IC tumor cells by the CTL, because of their low level of MHC class I expression (Supplementary Fig. S2D). As expected, B16-fucci Δ IC did not upregulate MHC class I molecules after exposure to IFN γ .

Because we could not evaluate the effect of IFN γ on tumor cells *in vivo* in this manner, we tested its effects directly on B16 tumor cells *in vitro*. As shown in Fig. 5, proliferation of B16-fucci cells, but not B16-fucci Δ IC cells, was inhibited completely when they were treated with IFN γ (Fig. 5A). These cells were arrested in G₁ (Fig. 5B), showing that IFN γ directly inhibits the growth of B16-fucci tumor cells through G₁ cell-cycle arrest.

Recently, it was reported that a combination of IFN γ and TNF α produced by CD4⁺ T cells can drive tumor cells into senescence by inducing G₀–G₁ cell-cycle arrest through the activation of p16INK4a (14). Therefore, we tested the effect of IFN γ and/or

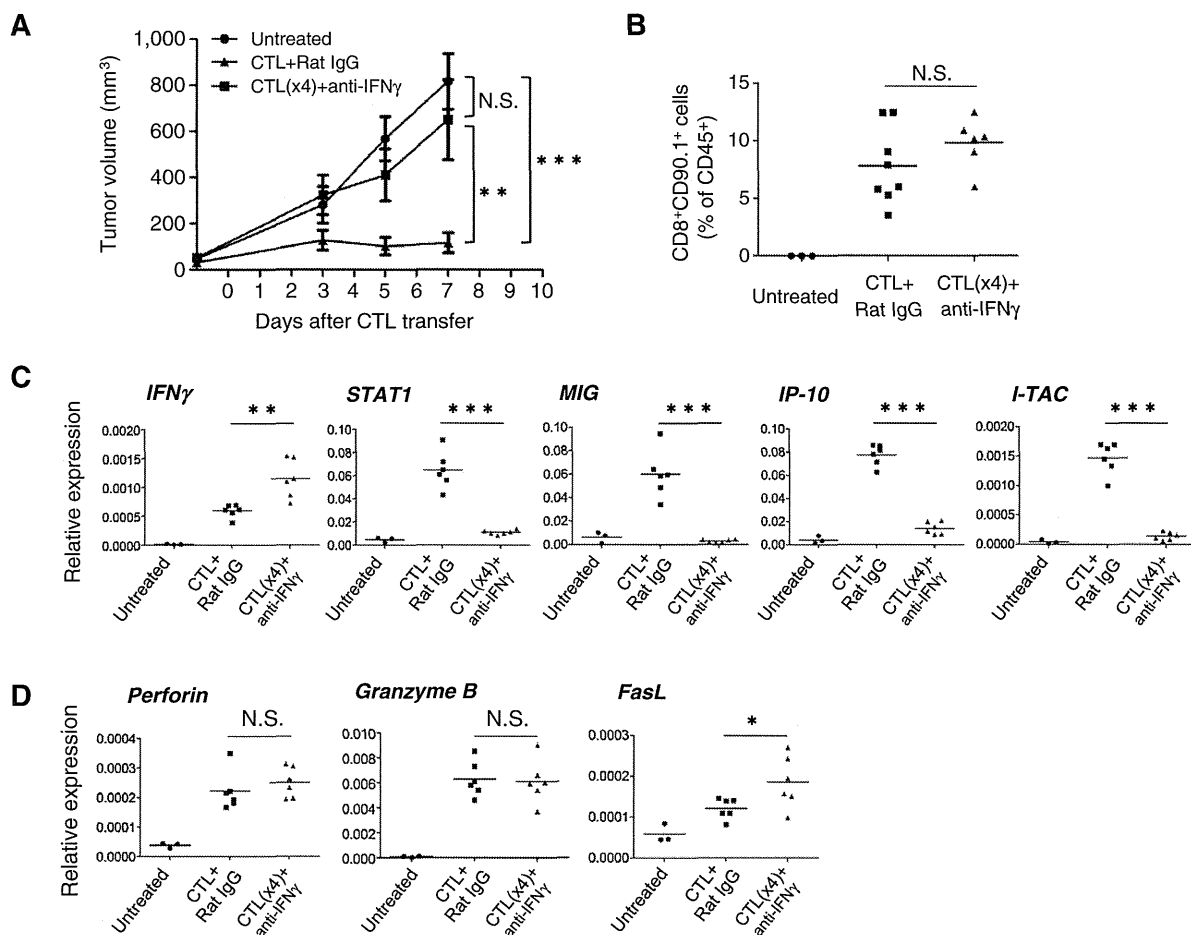


Figure 3. IFN γ is critical for tumor growth inhibition. A, C57BL/6 mice were injected with B16-fucci tumor cells. Tumor-bearing mice ($n = 5$) were treated as described in Fig. 1, and anti-IFN γ or control rat IgG antibodies were injected intraperitoneally on days 0 and 2 after CTL transfer. Tumor volumes were measured on days 3, 5, and 7 after CTL transfer ($n = 5$). B, the frequency of CTLs (CD45⁺ CD90.1⁺ CD8⁺) was assessed by flow cytometry. Tumors were harvested from each group on day 3 after CTL transfer. C and D, total RNA was isolated from tumor tissues and reverse-transcribed into cDNA. Expression of IFN γ -related genes (IFN γ , STAT1, MIG, IP-10, and I-TAC; C) and cytotoxicity-related genes (Perforin, Granzyme B, and FasL; D) was determined by qRT-PCR. GAPDH was used as an internal control. Samples were compared using an unpaired, two-tailed Student t test (*, $P < 0.05$; **, $P < 0.01$; and ***, $P < 0.001$; N.S., not statistically significant).

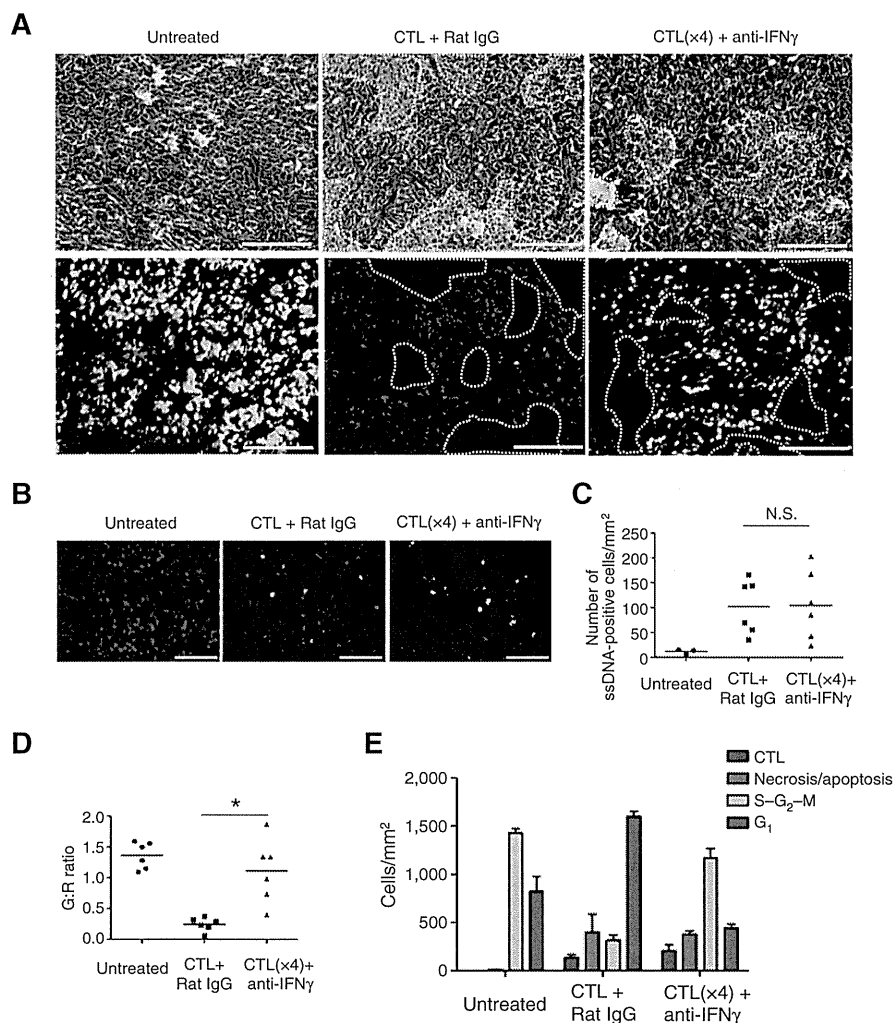
TNF α on B16 tumor cells. Whereas IFN γ alone inhibited cell proliferation by G₁ arrest, TNF α alone had a limited inhibitory effect on B16 proliferation even at a high concentration (10 ng/mL; Supplementary Fig. S3). When B16 tumor cells were cultured in the presence of both IFN γ and TNF α at a high concentration, a synergistic effect on cell growth inhibition and cell senescence was observed (Supplementary Fig. S3).

IFN γ production by transferred CTLs induces G₁ cell-cycle arrest by a mechanism involving Skp2/p27-related cell-cycle regulation

We next investigated the mechanism of G₁ cell-cycle arrest by IFN γ . B16-fucci tumor tissues were harvested from untreated mice, ACT mice treated with rat IgG, or ACT mice treated with anti-IFN γ mAb on day 3 after CTL transfer. Proteins were extracted from each tissue for Western blot analysis. As shown in Fig. 6A, downstream of IFN γ signaling, STAT1 was phosphorylated in

tumors from ACT mice treated with rat IgG, but not in tumors from anti-IFN γ mAb-treated ACT mice. To confirm the gene expression data that *Skp2* was significantly downregulated in tumors from ACT mice (Fig. 1B and C), we examined the protein expression of Skp2. As shown in Fig. 6A, Skp2 expression was suppressed in tumors from control ACT mice, but not in those from mice treated with anti-IFN γ mAb. Conversely, the cyclin-dependent kinase inhibitor (CKI) p27 accumulated in the former but not in the latter. We also investigated the ataxia telangiectasia mutated (ATM)-p53-p21 pathway involved in G₁ cell-cycle arrest following DNA damage. We found that ATM was not upregulated as a result of CTL therapy, p53 was not activated, and no subsequent accumulation of p21 was observed. This shows that the ATM-p53-p21 pathway is not involved in this model (Fig. 6A). We also investigated the expression of these molecules *in vitro* (Fig. 6B). B16-fucci and B16-fucci Δ IC tumor cells were treated with 10 U/mL IFN γ and

Matsushita et al.

**Figure 4.**

CTLs block tumor growth by both lytic activity and IFN γ -dependent cell-cycle arrest. A, B16-fucci tumor-bearing mice ($n = 3$) were treated as described in Fig. 3. Hematoxylin and eosin (top) and fluorescence microscopy images (bottom) of frozen tumor sections on day 3 are shown. Dotted yellow lines, necrotic areas. Scale bars, 200 μ m. B, apoptotic cells positive for ssDNA are shown in fluorescence microscopy images on day 3. Cells were counterstained with DAPI. Scale bars, 100 μ m. C, quantification of ssDNA-positive cells within tumors. Numbers of ssDNA-positive cells were counted in five random fields of view. Data are expressed as the means \pm SE of untreated mice ($n = 3$) and ACT mice injected with rat IgG ($n = 6$) or anti-IFN γ mAb ($n = 6$). D, analysis of the cell cycle was performed by calculating the G:R ratio in fluorescence images ($n = 6$ per group). E, the number of CTLs, tumor cells in necrotic areas, and tumor cells in G₁ or S-G₂-M. The number of cells in necrotic areas was estimated by calculating the surface area of the region using BZ-HIM software (Keyence). Total number of cells in at least three random fields of view (per mm²) is shown. Representative data of 3 mice for each group are given. Samples were compared using an unpaired, two-tailed Student t test (*, $P < 0.01$; N.S., not statistically significant).

harvested at the indicated times. STAT1 phosphorylation was observed at early time points (15 and 30 minutes after IFN γ treatment) in B16-fucci, but not in B16-fucci Δ IC. Skp2 expression was downregulated gradually, and p27 accumulated by 48 hours after IFN γ treatment in B16-fucci but not in B16-fucci Δ IC cells (Fig. 6B). We confirmed that the ATM-p53-p21 pathway was also not involved in G₁ cell-cycle arrest *in vitro*. These results suggest that G₁ cell-cycle arrest by CTL therapy is likely due to Skp2/p27-related cell-cycle regulation by IFN γ .

Inhibition of FBL3 cell proliferation by IFN γ

We next investigated whether proliferation of other murine cell lines is inhibited by IFN γ . FBL3, p815, CT26, 3LL, and EL4 tumor cells were treated with IFN γ (10 U or 100 U/mL) for 4 to 6 days (Fig. 7A). The proliferation of FBL3 tumor cells was inhibited by IFN γ treatment in a manner similar to that of B16 tumor cells. The proliferation of P815, CT26, and 3LL tumor cells was moderately inhibited. No inhibition was observed in IFN γ -treated EL4 tumor cells. In Western blot analyses, using tumor lysates from FBL3 and EL4 tumors at the indicated time point, Stat1 phosphorylation was observed in FBL3 lysates, but the phosphorylation was very

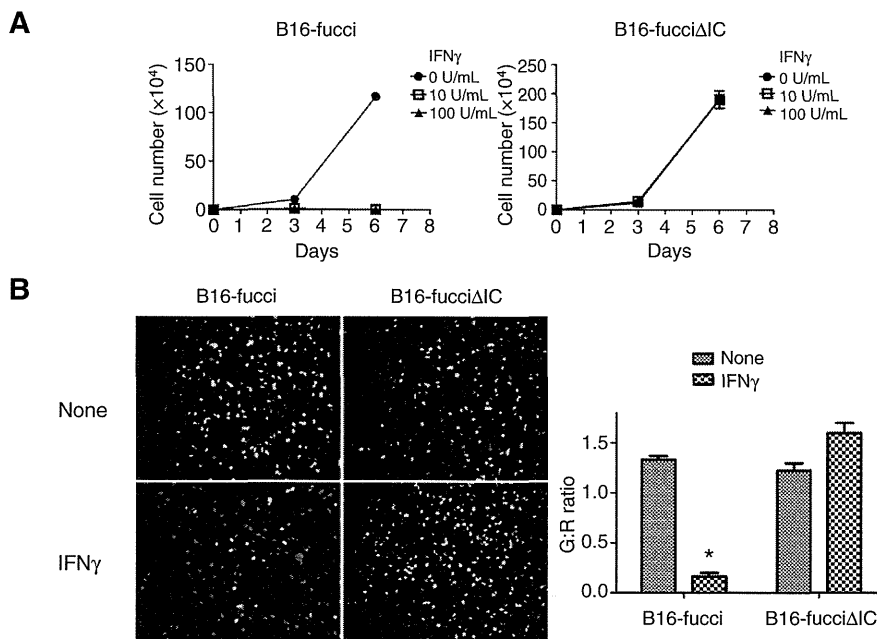
weak in EL4 tumor lysates. Skp2 expression was downregulated 24 to 48 hours after IFN γ treatment in FBL3 but not in EL4 tumors, and p27 accumulated (Fig. 7B). Again, the ATM-p53-p21 pathway was not involved. These results suggest that inhibition of FBL3 tumor cell proliferation by IFN γ might involve Skp2/p27-related cell-cycle regulation, as in B16.

Discussion

In this study, we demonstrated that the mechanism of tumor growth inhibition by adoptive CTL therapy was largely dependent on IFN γ -induced G₁ cell-cycle arrest rather than on tumor cell lysis. In microarray analysis, the upregulation of genes related to CD8⁺ T cells, the MHC class I pathway, IFN γ signaling, cytotoxic effector molecules, and others was observed in tumors from ACT mice. At the same time, a decrease was found in the expression of some genes positively regulating the cell cycle in these tumors. Therefore, we focused on cell-cycle control in the B16 adoptive immunotherapy model and used the fucci system, which allows the visualization of cell-cycle stage of tumor cells *in situ* in mice receiving CTL.

Figure 5.

IFN γ directly inhibits tumor cell growth through G₁ cell-cycle arrest. A, proliferation of B16-fucci cells or B16-fucci expressing an IFN γ receptor lacking the intracellular component (B16-fucci Δ IC) was assessed after exposure to IFN γ (10 U/mL) for 6 days. B, B16-fucci or B16-fucci Δ IC cells were incubated with IFN γ (10 U/mL). Two days later, the cell-cycle state was determined by fluorescence microscopy (left). Original magnification, $\times 200$. The G:R ratio in fluorescence images is shown ($n = 2$ per group; right). Samples were compared using an unpaired, two-tailed Student t test (*, $P < 0.01$).



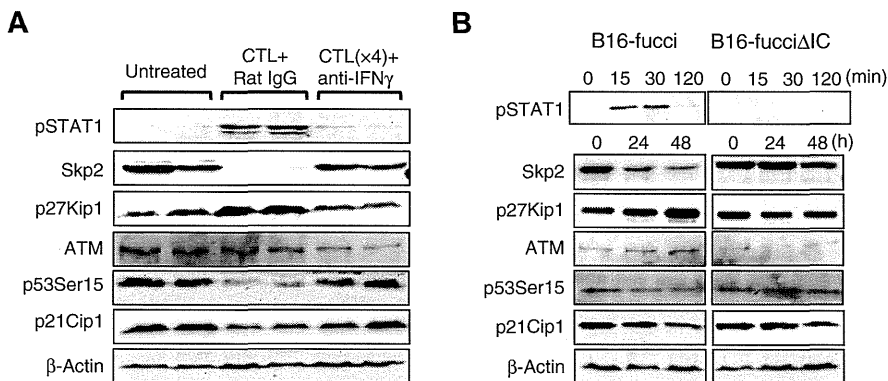
Histologic analysis following ACT showed that the number of CTLs in the tumor was far lower than that of tumor cells. On average, only 140 CTLs per mm² tumor tissue on day 3 after transfer were found. In contrast, this area contained 1,911 tumor cells (both green and red cells). Thus, it seems *a priori* unlikely that this small number of CTLs infiltrating the tumor would be sufficient to prevent tumor growth by direct cytotoxicity 3 to 7 days after CTL injection. Consistent with this observation, we also found that the area of the tumor undergoing necrosis/apoptosis was relatively small. Instead, a larger area consisting of tumor cells had undergone cell-cycle arrest at G₁. Therefore, transient tumor suppression from days 3 to 7 seems to be largely due to cell-cycle arrest rather than due to CTL killing. Using mAbs that neutralize IFN γ and completely block IFN γ signaling, we demonstrated that IFN γ is required for tumor growth inhibition and G₁ cell-cycle arrest but not for CTL killing. Thus, IFN γ -dependent G₁ cell-cycle arrest makes a major contribution to tumor growth suppression in this model. This would explain why tumor growth was suppressed despite the low ratio of CTLs to tumor cells in this system, and how

T cells can suppress the growth of bystander tumor cells that may not express the target antigen. This could also explain some examples to tumor suppression by CD4⁺ T cells that can also make IFN γ even if they are not lytic and even if the tumor is MHC class II negative, as long as antigen-presenting cells are infiltrating and can present antigen, as the soluble IFN γ can target neighboring cells.

IFN γ inhibits cell proliferation via cell type-specific pathways that involve CKIs, such as p21Cip1 (29, 30) and p27Kip1 (31, 32). It has been shown that STAT1 interacts directly with cyclin D1/Cdk4 and mediates the cell-cycle arrest of human U3A cells (33). Here, we investigated the involvement of CKIs in G₁ cell-cycle arrest, and found that p27Kip1, but not p21Cip1, accumulated in B16 tumor cells following CTL therapy *in vivo* or IFN γ treatment *in vitro*. Another CKI, p16, is involved in senescence-like G₁ cell-cycle arrest (14), but this factor is not expressed in B16 tumor cells due to a p16^{Ink4a} exon1 α deletion (34). Thus, p27Kip1 appeared to be the major CKI involved in G₁ arrest in this model. Skp2 is an oncogene; Skp2 inactivation induces cell senescence independent

Figure 6.

G₁ cell-cycle arrest by ACT was mediated by IFN γ -dependent Skp2/p27-related cell-cycle regulation. A, B16-fucci tumors were harvested from untreated or ACT mice given control rat IgG or anti-IFN γ mAb on day 3 after CTL transfer. Protein extracts (50 μ g) from tumor tissues in each group were used for immunoblotting of the indicated proteins. B, protein extracts from B16-fucci or B16-fucci Δ IC cells treated with IFN γ (10 U/mL) for the indicated time were used for immunoblotting of the indicated proteins.



Matsushita et al.

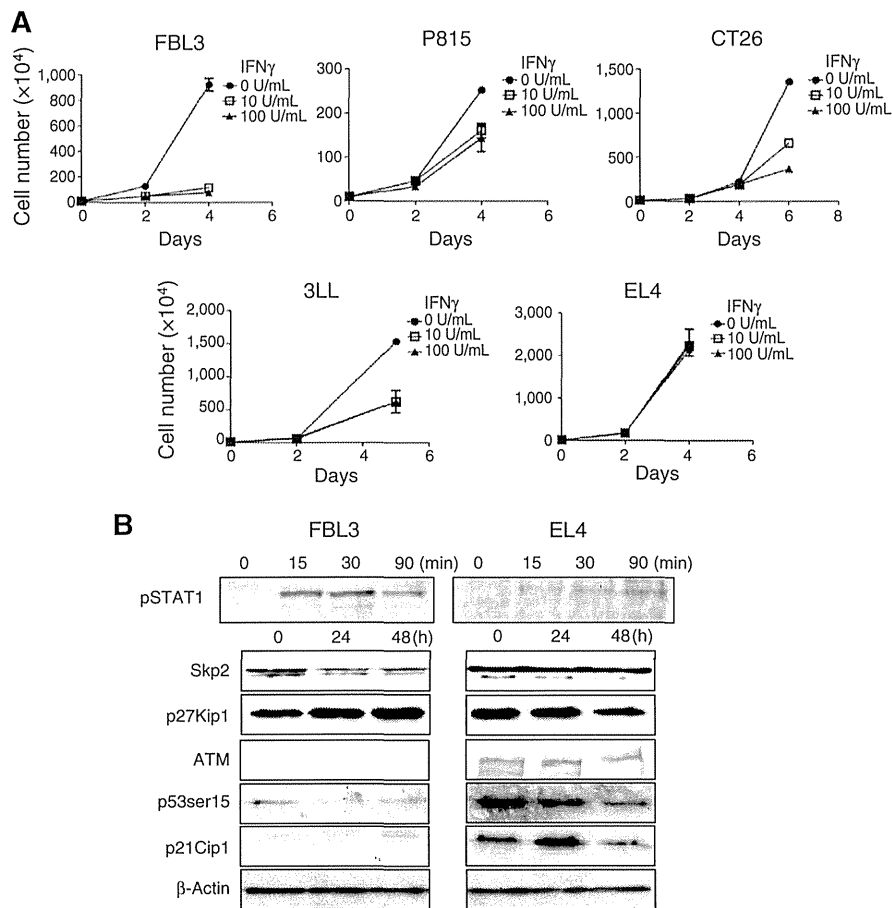


Figure 7. Inhibition of cell proliferation by IFN γ in other murine cell lines. A, proliferation of FBL3, P815, CT26, 3LL, and EL4 cells after treatment with IFN γ (10 or 100 U/mL) for 4 to 6 days. B, protein extracts from FBL3 and EL4 cells treated with IFN γ (10 U/mL) for the indicated time were used for immunoblotting of the indicated proteins.

of the p53 pathway (35). STAT1 has been shown to repress *Skp2* gene transcription by binding to its promoter region and stabilizing p27Kip1 in Ras-transformed cells (36). In this report, we showed that Skp2 expression was downregulated after either CTL therapy or IFN γ treatment; thus, STAT1 may repress Skp2 expression and promote p27Kip1 stabilization.

G₁ cell-cycle arrest is also known to be induced by ATM-dependent activation of p53 and induction of p21Cip1 (37). Because ATM is a key molecule in the cellular response to DNA damage (38), we investigated its expression by Western blot analysis. We found that the ATM protein was not highly expressed in the tumor after CTL therapy. We also confirmed this finding *in vitro* in B16 cells cultured with IFN γ . Furthermore, p53 was not phosphorylated at Ser15, and the CKI p21Cip1, which is downstream of phospho-p53 (Ser15), was not upregulated. Therefore, we conclude that ATM expression and the subsequent activation of the phospho-p53–p21 pathway was not involved in this model.

We tested the effect of IFN γ on other murine tumor cell lines, and found that the proliferation of FBL-3 cells was strongly inhibited by IFN γ , similar to that of the B16 tumor cells. On the other hand, EL-4 cells were insensitive to IFN γ , whereas p815, CT26, and 3LL cells were moderately sensitive. IFN γ sensitivity and the mechanisms involved in the inhibition of cell prolifer-

ation may differ in different tumor cell lines. It is important to know whether IFN γ insensitivity is due to the downregulation of IFN γ receptors on these tumors, or defects in their IFN γ signal transduction.

Braumuller and colleagues (14) reported that IFN γ together with TNF α reduced the proliferation of different cancer cell lines in both mice and humans. Here, we showed that the combination of IFN γ and TNF α strongly inhibited B16 tumor cell proliferation and induced cell senescence (Supplementary Fig. S3). Because pmel-1 CTLs produce large amounts of IFN γ , but not TNF α , when they are cultured with B16 tumor cells *in vitro* (Supplementary Fig. S4), and IFN γ alone is enough to suppress tumor cell proliferation (Supplementary Fig. S3), the transient suppression of tumor growth from days 3 to 7 *in vivo* in this model may be entirely due to IFN γ , as there is only a small amount of TNF α at the tumor site. Th1 CD4⁺ T cells or Toll-like receptor (TLR)-stimulated macrophages might be able to produce enough TNF α , but these cells are not present in our system. Alternatively, a strategy to induce polyfunctional CD8⁺ T cells producing IFN γ , TNF α , and IL2 might be important to enhance further the antitumor effects in this model (39, 40).

IFN γ is a critical molecule in cancer immunosurveillance or immunoeediting in primary mouse tumor models (41–44). In our study, as long as high concentrations of IFN γ were present

in the tumor, its growth was controlled through G₁ arrest (Supplementary Fig. S1). Thus, our study suggests that deregulation of the cell cycle due to insufficient availability of IFN γ or IFN γ insensitivity developed by tumor cells may be one mechanism by which tumor cells escape from CTL therapy (Supplementary Figs. S1 and S2).

Our study indicates that a small number of infiltrated CTLs can cause a large number of tumor cells to arrest in G₁ rather than dying. On the basis of this finding, we propose that the development of an appropriate strategy to maintain tumor cells in a quiescent, dormant state for extended periods (immunotherapy-induced equilibrium/dormancy), or to induce apoptosis/senescence, would be highly desirable.

Disclosure of Potential Conflicts of Interest

No potential conflicts of interest were disclosed.

Authors' Contributions

Conception and design: H. Matsushita, R. Maekawa, K. Kakimi

Development of methodology: M. Tomura, K. Kakimi

Acquisition of data (provided animals, acquired and managed patients, provided facilities, etc.): H. Matsushita, A. Hosoi, S. Ueha, J. Abe, N. Fujieda, R. Maekawa, O. Ohara, K. Kakimi

Analysis and interpretation of data (e.g., statistical analysis, biostatistics, computational analysis): H. Matsushita, A. Hosoi, S. Ueha, N. Fujieda, O. Ohara, K. Kakimi

Writing, review, and/or revision of the manuscript: H. Matsushita, K. Kakimi

Administrative, technical, or material support (i.e., reporting or organizing data, constructing databases): O. Ohara

Study supervision: K. Matsushima, K. Kakimi

Acknowledgments

The authors thank Dr. N. Restifo (National Cancer Institute) for providing the B16F10 tumor cell line, Dr. A. Miyawaki (RIKEN, Wako) for the Fucci system, and Mr. K. Sato (Kazusa DNA Research Institute) for excellent technical assistance in gene expression analysis.

Grant Support

This study was supported in part by a Grant-in-Aid for Scientific Research of the Ministry of Education, Culture, Sports, Science and Technology of Japan (K. Kakimi).

The costs of publication of this article were defrayed in part by the payment of page charges. This article must therefore be hereby marked *advertisement* in accordance with 18 U.S.C. Section 1734 solely to indicate this fact.

Received May 16, 2014; revised July 22, 2014; accepted August 5, 2014; published OnlineFirst August 15, 2014.

References

- Rosenberg SA, Restifo NP, Yang JC, Morgan RA, Dudley ME. Adoptive cell transfer: a clinical path to effective cancer immunotherapy. *Nat Rev Cancer* 2008;8:299–308.
- Morgan RA, Dudley ME, Wunderlich JR, Hughes MS, Yang JC, Sherry RM, et al. Cancer regression in patients after transfer of genetically engineered lymphocytes. *Science* 2006;314:126–9.
- Brenner MK, Heslop HE. Adoptive T cell therapy of cancer. *Curr Opin Immunol* 2010;22:251–7.
- Kalos M, Levine BL, Porter DL, Katz S, Grupp SA, Bagg A, et al. T cells with chimeric antigen receptors have potent antitumor effects and can establish memory in patients with advanced leukemia. *Sci Transl Med* 2011;3:95ra73.
- Robbins PF, Morgan RA, Feldman SA, Yang JC, Sherry RM, Dudley ME, et al. Tumor regression in patients with metastatic synovial cell sarcoma and melanoma using genetically engineered lymphocytes reactive with NY-ESO-1. *J Clin Oncol* 2011;29:917–24.
- Vierboom MP, Nijman HW, Offringa R, van der Voort EI, van Hall T, van den Broek L, et al. Tumor eradication by wild-type p53-specific cytotoxic T lymphocytes. *J Exp Med* 1997;186:695–704.
- Hanson HL, Donermeyer DL, Ikeda H, White JM, Shankaran V, Old LJ, et al. Eradication of established tumors by CD8+ T cell adoptive immunotherapy. *Immunity* 2000;13:265–76.
- Mukherjee P, Ginardi AR, Tindler TL, Sterner CJ, Gendler SJ. MUC1-specific cytotoxic T lymphocytes eradicate tumors when adoptively transferred *in vivo*. *Clin Cancer Res* 2001;7:848s–55s.
- Kagi D, Vignaux F, Ledermann B, Burki K, Depraetere V, Nagata S, et al. Fas and perforin pathways as major mechanisms of T cell-mediated cytotoxicity. *Science* 1994;265:528–30.
- Spiotto MT, Rowley DA, Schreiber H. Bystander elimination of antigen loss variants in established tumors. *Nat Med* 2004;10:294–8.
- Breart B, Lemaître F, Celli S, Boussou P. Two-photon imaging of intratumoral CD8+ T cell cytotoxic activity during adoptive T cell therapy in mice. *J Clin Invest* 2008;118:1390–7.
- Zhang B, Karrison T, Rowley DA, Schreiber H. IFN- γ - and TNF-dependent bystander eradication of antigen-loss variants in established mouse cancers. *J Clin Invest* 2008;118:1398–404.
- Muller-Hermelink N, Braumüller H, Pichler B, Wieder T, Mailhammer R, Schaak K, et al. TNFR1 signaling and IFN- γ signaling determine whether T cells induce tumor dormancy or promote multistage carcinogenesis. *Cancer Cell* 2008;13:507–18.
- Braumüller H, Wieder T, Brenner E, Assmann S, Hahn M, Alkhaled M, et al. T-helper-1-cell cytokines drive cancer into senescence. *Nature* 2013;494:361–5.
- Dunn GP, Koebel CM, Schreiber RD. Interferons, immunity and cancer immunoeediting. *Nat Rev Immunol* 2006;6:836–48.
- Winter H, Hu HM, McClain K, Urba WJ, Fox BA. Immunotherapy of melanoma: a dichotomy in the requirement for IFN- γ in vaccine-induced antitumor immunity versus adoptive immunotherapy. *J Immunol* 2001;166:7370–80.
- Liao F, Rabin RL, Yannelli JR, Koniaris LG, Vanguri P, Farber JM. Human Mig chemokine: biochemical and functional characterization. *J Exp Med* 1995;182:1301–14.
- Luster AD, Leder P. IP-10, a -C-X-C- chemokine, elicits a potent thymus-dependent antitumor response *in vivo*. *J Exp Med* 1993;178:1057–65.
- Cole KE, Strick CA, Paradis TJ, Ogborne KT, Loetscher M, Gladue RP, et al. Interferon-inducible T cell alpha chemoattractant (I-TAC): a novel non-ELR CXC chemokine with potent activity on activated T cells through selective high affinity binding to CXCR3. *J Exp Med* 1998;187:2009–21.
- Bromberg JF, Horvath CM, Wen Z, Schreiber RD, Darnell JE Jr. Transcriptionally active Stat1 is required for the antiproliferative effects of both interferon alpha and interferon gamma. *Proc Natl Acad Sci U S A* 1996;93:7673–8.
- Chin YE, Kitagawa M, Su WC, You ZH, Iwamoto Y, Fu XY. Cell growth arrest and induction of cyclin-dependent kinase inhibitor p21 WAF1/CIP1 mediated by STAT1. *Science* 1996;272:719–22.
- Meurs E, Chong K, Galabru J, Thomas NS, Kerr IM, Williams BR, et al. Molecular cloning and characterization of the human double-stranded RNA-activated protein kinase induced by interferon. *Cell* 1990;62:379–90.
- Deiss LP, Feinstein E, Berissi H, Cohen O, Kimchi A. Identification of a novel serine/threonine kinase and a novel 15-kD protein as potential mediators of the gamma interferon-induced cell death. *Genes Dev* 1995;9:15–30.
- Noji S, Hosoi A, Takeda K, Matsushita H, Morishita Y, Seto Y, et al. Targeting spatiotemporal expression of CD137 on tumor-infiltrating cytotoxic T lymphocytes as a novel strategy for agonistic antibody therapy. *J Immunother* 2012;35:460–72.
- Sakaue-Sawano A, Kurokawa H, Morimura T, Hanyu A, Hama H, Osawa H, et al. Visualizing spatiotemporal dynamics of multicellular cell-cycle progression. *Cell* 2008;132:487–98.